Material assembly by droplet drying: From mechanics

theories to applications

Ziyu Chen, Kangyi Peng, Baoxing Xu*

Department of Mechanical and Aerospace Engineering, University of Virginia, Charlottesville, VA 22904,

USA

* Corresponding author: bx4c@virginia.edu

Abstract

Evaporation of droplet composed of insoluble materials provides a low-cost and facile route for assembling

materials and structures in a wide spectrum of functionalities down to the nanoscale and also serves as a

basis for innovating ink-solution based future manufacturing technologies. This review summarizes the

fundamental mechanics theories of material assembly by droplet drying on both solid and liquid substrates

and in a fully suspended air environment. The evolution of assembly patterns, material deformation and

liquid flow during droplet drying and its response to external stimuli ranging from solution surfactant and

pH value, surface geometric pattern and wettability, drying temperature, pressure environment, to electrical

field has been highlighted to elucidate the coupling mechanisms between solid materials and liquid solutions

and the manipulation strategies to material assembly through an either active or passive means. The recent

progress in ink-based printing technologies with selected examples is also presented to illustrate the

immediate applications of droplet drying with a focus on printing electronic sensors and biomedical devices.

The remaining challenges and emerging opportunities are discussed.

Key words

Droplet drying; Material assembly; Theory; Ink-based printing; Sensors.

Introduction

Material assembly by droplet drying has been a subject of significant research interest over the last two

decades thanks to its broad applications such as inkjet printing, 1, 2 surface coating, 3 biosensors, 4, 5 and

diagnostics.^{6, 7} Generally speaking, evaporation of droplet composed of insoluble materials can be

summarized to three categorizations on the basis of evaporation substrate: solid substrate (liquid-solid

system), liquid substrate (liquid-liquid system), and suspended in air (liquid-air system).

The evaporation of droplets containing insoluble particles on solid substrates, often referred to as colloidal

sessile droplet evaporation, has been the subject of numerous studies due to its significant scientific and

industrial applications.8 For example, one of the seminal work demonstrated that the convective outward

flow during evaporation drives the particles to migrate toward the pinned contact line, resulting in a ring-

like deposition pattern, commonly referred to as the "coffee ring" effect.^{9, 10} Studies on the drying of colloidal sessile droplets have revealed the existence of various mechanisms that influence the final particle distribution, including internal flow dynamics, ^{11, 12} evaporation dynamics, ¹³ evolution of droplet profiles, ^{14, 15} and interparticle and interfacial interactions. ^{16, 17} The dominative role among these mechanisms can be played by manipulating key controlling factors such as solute size and concentration, base fluid composition, environmental conditions, among others. The control and reproducibility of the deposition pattern currently remain a great challenge due to the associated contact angle hysteresis with the inhomogeneity and roughness of conventional solid substrate surfaces.

Compared to droplet drying on solid substrates, the liquid substrate is more conducive to particle assembly due to its deformability and flexibility, and as a result the structures formed on liquid substrate are more easily transferred than those formed on solid substrates. ¹⁸⁻²⁰ Most of the work for material assembly largely focuses on droplet morphology in equilibrium^{21, 22} and contact line dynamics during droplet drying. ^{23, 24} In fundamental, the spreading of droplets on solid substrates often follows the Tanner's law, ²⁵⁻²⁷ that could be altered by adjusting liquid and solid properties, wetting scenarios, and early time dynamics. By contrast, the most critical factor influencing droplet drying on an immiscible liquid substrate is the interfacial tension between the two liquids. This tension arises from the attractive and repulsive forces between the molecules at the interface and determines the spreading behavior of the droplet. When the droplet is placed on the surface of the immiscible liquid, it spreads until the interfacial tension between the two liquids is balanced by the capillary forces of the droplet. The interface characteristics play a vital role in governing the dynamics, with perfectly rigid and flat substrates resulting in the classical Young's equation. In liquid substrate, the normal force component can deform the liquid-liquid interface, resulting in a lens shape. The state of equilibrium for this lens can be determined using Neumann's triangles. ^{28, 29}

In terms of material assembly by drying of colloidal droplets in fully suspended air, it plays a crucial role in a wide range of industrial applications, including energy storage,³⁰ spray cooling,³¹ and wastewater treatment.³² Current studies on the evaporation of suspended droplets primarily focus on the self-assembly of materials within the droplets due to the simplicity of their evaporation mode. The structures assembled after drying typically depend on the desired materials.³³ For colloidal particles, the morphology depends on Péclet number determined by dominant transport mechanism - diffusive or convective. For example, slow drying with diffusive transport leads to spherical dense particles, while fast drying with convective transport results in shell formation, causing doughnuts, shriveled, or hollow particles. High Péclet number is necessary but not sufficient for shell formation.^{34, 35} In contrast to colloidal particles that typically do not undergo mechanical deformation, two-dimensional (2D) materials and one- dimensional (1D) materials can readily bend and fold when assembled through evaporative drying.³⁶⁻³⁸ Needless to say, the shape, size and material properties of 2D materials and 1D materials play a crucial role in the bulk forms after drying.

This work aims to provide a comprehensive overview of the recent progress for the material assembly by droplet drying. Droplet drying in solid and liquid substrates and suspended air environments from theoretical model development to applications will be reviewed. The mechanics and mechanisms of material assembly in these three systems and the assembled pattern morphologies are discussed in detail. The typical applications in ink-based printing technologies and printing of wearable sensors by droplet drying are also highlighted. It is important to mention that the droplets discussed in this review exclusively pertain to non-reactive systems. When reactive components are introduced, such as chemically reactive particles or reactive solvents, the drying can result in unintended chemical reactions, alterations in particle properties, or modifications to the assembly dynamics³⁹⁻⁴¹, which is out of scope in this review.

Fundamental mechanics theory of droplet drying: a brief overview

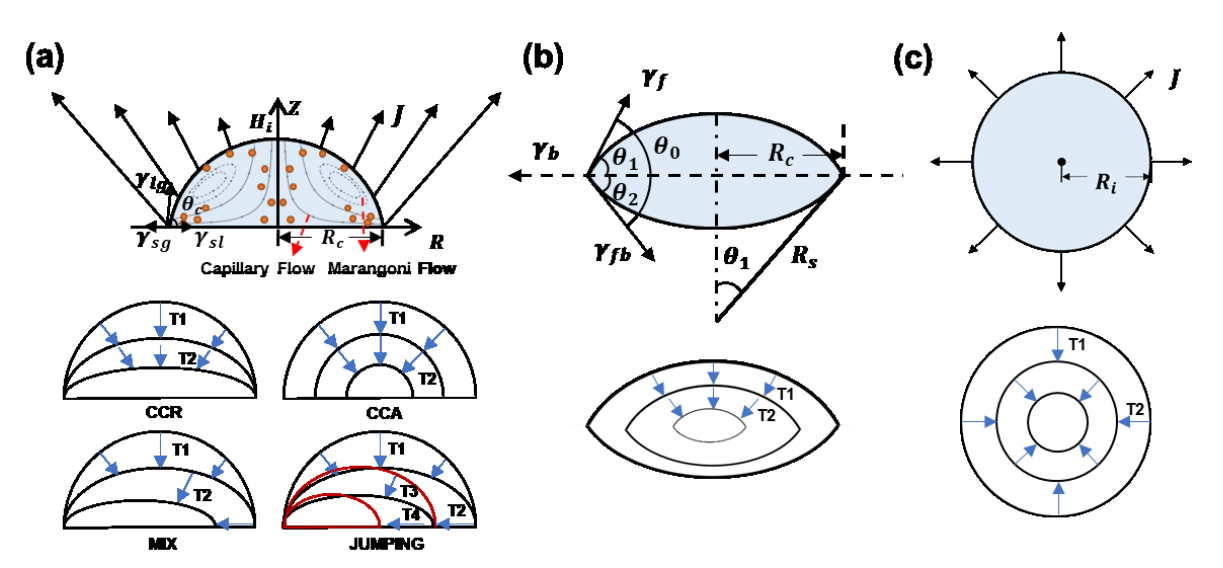


FIGURE 1 Fundamental mechanics theory of droplet drying. (a) Schematic of the sessile droplet with initial height (H_i) , contact radius (R_c) , and contact angle (θ_c) . (b) Schematic of the droplet evaporating on another liquid surface, where R_c , R_s , θ_1 , θ_2 is the contact radius, the upper spherical radius, the upper spherical cap angle, and the lower spherical cap angle, respectively. (c) Schematic of the evaporation of air suspended droplets with initial radius (R_i) .

Drying on a solid substrate

Sessile droplets are characterized by their initial height (H), contact radius (R), and contact angle (θ_c) , and are liquid droplets that have been deposited on a solid substrate, where the contact line restricts the wetted area between the liquid and the solid surface. The evaporation of sessile droplets typically exhibits four modes (**Figure 1a**), including the constant contact radius (CCR) mode, the constant contact angle (CCA) mode, the mixed mode, and the 'stick-slip' (jumping) mode. 42-44 Generally, the evaporation mode on hydrophobic solid substrates is the CCA mode, while on hydrophilic solid substrates, the CCR mode is more prevalent. The Young's equation describes the equilibrium contact angle of a droplet on a solid surface, which is given by:

$$\cos\theta_c = (\gamma_{sv} - \gamma_{sl})/\gamma_{lv} \tag{1}$$

where θ_c is the contact angle, γ_{sv} is the solid-vapor surface tension, γ_{sl} is the solid-liquid surface tension, and γ_{lv} is the liquid-vapor surface tension. The competition between the forces acting on each particle at the contact line leads to particle deposition near the contact line. When the inward surface tension surpasses all other forces during evaporation, contact line depinning takes place, and the evaporation mode transitions gradually from CCR to CCA and/or MIX. Notably, another significant element influencing the deposition pattern is the flow field within the sessile droplet. The two most typical flows are capillary flow and Marangoni flow. The liquid travels radially to the edge of the droplet to refill the evaporated liquid at the edge because the evaporation rate at the contact line is higher than the core portion of the droplet. This flow is known as capillary flow (Figure 1a), which often happens in the CCR mode and is given by 45, 46:

$$Q(r) = \frac{2R_c D\Delta c}{\pi \rho} \left[\sqrt{1 - (r/R_c)^2} - (1 - (r/R_c)^2)^2 \right]$$
 (2)

with Q(r) the volume flow at a distance r from the center of the droplet, R_c the contact radius, D the diffusion coefficient of vapor in air, and Δc the disparity between the concentration of saturated vapor immediately above the interface between the liquid and air, and the concentration of ambient vapor far from the droplet. A surface tension gradient along the droplet's free surface is what propels Marangoni flow. The local temperature and the uneven distribution of concentration at the liquid-vapor interface are the two main contributors to this surface tension gradient. Marangoni convection occurs when liquid in evaporating droplets tends to move from areas of lower surface tension to areas of greater surface tension. The Marangoni number Ma can be used to quantify Marangoni flow. This number is defined as the ratio between the advective flow driven by the Marangoni effect and the diffusive transport of the property responsible for generating the surface tension gradient. In its most generic form, the Ma number provides a measure of the strength Marangoni flow:

$$Ma = UL/D_{\chi} \tag{3}$$

where L is the length scale of the concentration gradient, and D_{χ} is the diffusion constant of variable χ , measured in terms of area per unit time. An estimate of the order of magnitude of the Marangoni flow U can be obtained using the ratio of the surface tension difference $\Delta \gamma$ to the liquid's dynamic viscosity μ . This equation describes how the gradient in surface tension drives the flow of the liquid within the droplet. Also, when the substrate was heated, Marangoni flow was shown to be more intense than capillary flow. In the case of cooled substrates, however, capillary flow is more significant than Marangoni flow.^{48, 49}

Drying on a liquid surface

When a droplet is positioned on mutually incompatible liquid substrates, the contact line at the liquid-liquid interface is more likely to shrink compared to that at the solid-liquid interface. This is due to the differences in surface energies between the two liquids, which result in a gradient of interfacial tension that drives the droplet to adopt a more spherical shape. As a result, the evaporation of droplets on mutually incompatible liquid substrates primarily follows the CCA mode (**Figure 1b**).²⁴ The Marangoni effect, which refers to the

flow of liquid caused by gradients in surface tension, is weak in this case due to the strong heat transfer in the liquid-liquid system. 50 As a result, evaporative convection dominates the particle dynamics at the liquid-gas interface. This can lead to the formation of convection currents that can transport particles within the droplet, affecting its evaporation rate and final shape. To determine the equilibrium state of a floating liquid on the surface of a denser liquid bath, it is necessary to consider various factors such as surface tension, intermolecular interaction between the floating liquid and the bath, as well as hydrostatic pressure. This is typically achieved through an analysis of the free energy per unit area, denoted as F, of the floating liquid film with thickness h. 22

$$F(h) = \gamma_f + \gamma_{fb} + P(h) + \frac{1}{2}\rho_f g\Delta h^2 \tag{4}$$

where γ_f and γ_{fb} are respectively the surface tension between the floating liquid and the gas and between the floating liquid and the bath, $\Delta = (\rho_b - \rho_f)/\rho_b$ and P(h) is the interaction energy per unit area through the thickness of the floating liquid. Besides, At the edge of the floating droplet lens, the equilibrium is given by the Neumann condition:⁵¹

$$\vec{\gamma}_b + \vec{\gamma}_f + \vec{\gamma}_{fb} = \vec{0} \tag{5}$$

The Neumann condition yields a direct expression for the contact angle of the lens, denoted as θ_0 in Figure 1b, as a function of the surface tension.

$$\cos\theta_0 = \frac{\gamma_b^2 - \gamma_f^2 - \gamma_{fb}^2}{2\gamma_f \gamma_{fb}} \tag{6}$$

Hence, different equilibrium states can be identified depending on the evolution of F(h) and the spreading parameter $S_{fb} = \gamma_b - \gamma_f - \gamma_{fb}$.

Drying in a suspended air environment

The evaporation process of the droplet suspended in air occurs in a concentric manner without the contact line pinning effect that is associated with solid surfaces, similar to the CCA mode (**Figure 1c**). In absence of a substrate, the evaporative flux from the droplet surface is uniform and directed radially outwards. In the diffusion-limited regime the evaporative mass flux J and the rate of mass loss from the droplet are separately given by⁵²

$$J = D\Delta c/R \tag{7}$$

$$\frac{dM}{dt} = -4\pi RD\Delta c \tag{8}$$

The famous R^2 law can be deduced by combing expressions (7) and (8):

$$R^2(t) = R_i^2 - 2\frac{D\Delta c}{\rho}t\tag{9}$$

Importantly, the evaporative flux from the surface of a freely suspended drop does not induce any flow inside the droplet. Instead, as the droplet loses mass through evaporation, the interface of the droplet gradually moves inward to compensate for the reduction in mass. Hence, The assembly of particles within the colloidal droplet suspended in air is mainly driven by the contraction of the droplet surface rather than the evaporation-

induced internal flow, and the influence of the liquid flow on the particles is almost negligible.^{33, 36} In other words, it is not the particles that get advected to the interface, but vice versa: the interface recedes inwards, assembling the particles together.

Compared with the assembly of materials on these above different substrates/environments, a very broad variety of one-dimensional (1D) and two-dimensional (2D) nanomaterials are also employed for their assembly into large-scale structures by leveraging uniqueness of droplet drying process because of potential applications in various fields. For example, droplet drying based printing and aerosol technique has been used to print 2D materials-enabled functional structures and devices. 53-55 In contrast to assembly of colloidal particles which are usually rigid and do not experience mechanical deformation during solution evaporation, 1D or 2D nanomaterials are highly susceptible to experience deformation, wrinkling, and folding along with the assembly. 56-58 This is due to very low out-of-plane mechanical flexibility associated with their high aspect ratio of geometric features. For instance, 1D nanomaterials, such as nanowires, are highly susceptible to bending or buckling during the drying process. For 2D materials like graphene, the formation of wrinkles or folds is expected as the droplet dries. Recently, an energy-based mechanics theory has been developed to describe the spontaneous mechanical deformation and assembly of 2D nanomaterials by droplet drying. Specifically, the deformation energy of 2D sheet can be defined as 36

$$E_{df} = \sum_{i=1}^{n} k_s \left(\theta_t^{(i)} - \pi\right)^2$$
 (10)

where k_s is the constant of rotational spring that aims to describe the out-of-plane mechanical deformation of 2D materials and θ_t is the rotation angle corresponding the magnitude of out-of-plane deformation. Also, the assembly energy is given by

$$E_{as} = \sum_{i=1}^{n_l} k_b^{(i)} A_{bind}^{(i)} \left[\sin \left(\theta_t^{c(i)} / 2 \right) - \sin \left(\theta_t^{(i)} / 2 \right) \right] H \left(\theta_t^{c(i)} - \theta_t^{(i)} \right)$$
(11)

where k_b is the constant of the mechanical slider that is implemented to describe the interactive binding energy in self-folding of a single 2D sheet or overlap of neighboring 2D sheets. $A_{bind}^{(i)}$ represents the deformed area of wrinkling and self-folding, $H(\theta_t^c - \theta_c)$ is the Heaviside function, and $H(\theta_t^c - \theta_c)=0$ at $\theta_t^c \geq \theta_t$, and $H(\theta_t^c - \theta_c)=1$ at $\theta_t^c < \theta_t$, where θ_t^c corresponds to the critical rotation angle of spring model, and at $\theta_t < \theta_t^c$, the associated two connected rigid parts of 2D sheets are considered to be close enough and the resultant binding energy needs to be considered. The theoretical analysis shows remarkable agreement with parallel coarse-grained computational simulation and independent experiments. This energy based theoretical model has also been extended to assemble composite particles with both 1D and 2D materials,³⁷ paving the foundation for assembling composite materials and structures by solution evaporation of droplets with a broad range of material compositions and their mixtures.

As direction validations to these theories, numerous simulations in colloidal droplet drying have been conducted from particle assembly to pattern formation down to the nanoscale. At the continuum scale, for example, bipolar coordinate-based models have been proposed to describe the capillary flow during colloidal droplet desiccation using the Stokes approach.⁵⁹⁻⁶¹ Finite element method has also been developed to compute velocity fields within evaporating droplets 12,62 When the suspended particles are taken into account in the droplet, various models and simulations are proposed to replicate two distinct situations during colloidal droplet desiccation: the formation of porous media and the development of strong interparticle bonds. For instance, some models employ partial differential equations (PDE) to simulate these systems. ⁶³, ⁶⁴ At the nanoscale, Monte Carlo algorithms and molecular dynamics simulations are frequently employed to simulate the molecular drying process and assembly physics. 65-67 For example, the Monte Carlo algorithm has been successfully validated for predicting the behavior of an ensemble of colloidal solid particles or coalescing liquid droplets suspended in a turbulent gas flow, as determined by the Reynolds Averaged Navier-Stokes approach (RANS).⁶⁸ Molecular dynamics simulations could provide the intricate dynamics and interactions among individual molecules during the drying process.⁶⁹ Coarse-grained models with a high-performance virtual force field between liquid and solid materials have also been developed to simultaneously simulate the dynamics and competition between mechanical deformation and assembly process of solid materials during evaporation.^{36, 37, 58} Simulations toward the potentially seamless integration with the rapid development of advanced computational algorithms such as machine learning could be an important topic in the study of material assembly by drying. 70, 71

Material assembly patterns and morphology evolutions

Assembly on a solid substrate

The evaporation of a colloidal droplet on a solid substrate results in the deposition of particles that can form intricate patterns, with the patterns being dependent on the evaporation mode. The deposition patterns can range from simple rings to more complex structures such as crack, fingers, dot-like and coffee rings. These patterns are influenced by factors such as the size and concentration of particles, the drying rate, and the presence of surfactants. Moreover, the assembly patterns formed by the particles in the droplet can be further manipulated by the materials present in the droplet. For instance, incorporating polymers, nanoparticles, or biomolecules into the droplet can influence the final assembly pattern. This manipulation can be achieved by altering the interaction between the particles and the substrate, resulting in the formation of specific structures. In addition to material manipulation, the environment in which the droplet dries can also play a crucial role in determining the assembly patterns. Factors such as temperature, humidity, and airflow can impact the rate and direction of the droplet's evaporation and, in turn, the final deposition pattern.

Evaporation mode dependent deposition patterns

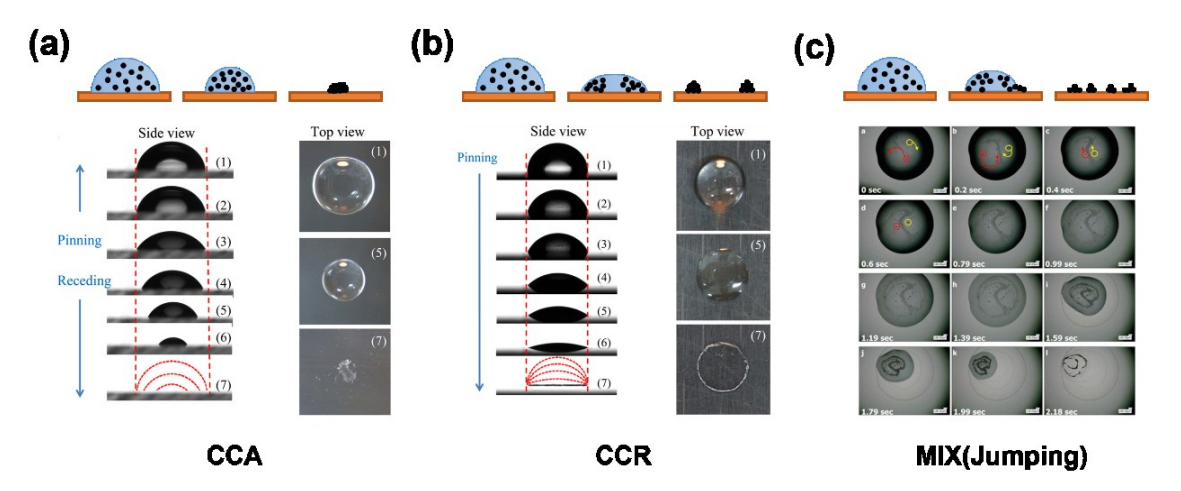


FIGURE 2 Classical deposition patterns of sessile droplet. (a) A dot-like pattern left after the drying of a sessile droplet following the CCA mode. Reproduced with permission. Chemical Society. (b) A coffee-ring left after the drying of a sessile droplet following the CCR mode. Reproduced with permission. Chemical Society. (c) Multiple concentric rings are formed on the substrate in the CCR mode. Adapted with permission. Chemical Society.

Upon complete evaporation of colloidal droplets in the CCA mode, a dot-like pattern can be most obtained on the substrate.^{73, 74} In the CCA mode, the wetted contact area decreases while the contact angle remains constant, resulting in a nonlinear decrease in volume over time (**Figure 2a**). Early in the drying process, particle adhesion to the substrate is inhibited due to the contraction of the contact line caused by evaporation. As evaporation continues, the particle concentration increases, and the particles begin to aggregate.⁷² The formation of this dot-like pattern is largely attributed to the CCA evaporation mode and inward Marangoni flow, which can move the particles to the center of the droplet during the drying process.⁷⁵ In the final stages of evaporation, as the contact angle narrows over time, Marangoni flow decreases and forms radially outward near the substrate.⁷³ However, given that the internal particle structure of the droplet has already been established at this point, the outward flow is unable to move the particles from the center to the edge.

In the CCR mode, as the height of the droplet decreases while maintaining its spherical cap shape and constant radius (**Figure 2b**), liquid must be supplied from the interior of the droplet to replace the liquid evaporating at the contact line, resulting in an outward capillary flow within the droplet driven by free surface energy. This flow carries suspended particles towards the edge of the droplet, leading to their deposition near the contact line. The formation of a coffee ring requires that several conditions are met. Firstly, the CCR evaporation pattern must be established. Secondly, the interaction of droplet size, particle concentration, evaporation rate, and the recirculating Marangoni flow, driven by the surface tension gradient, must be considered. The particle concentration within a droplet of a given size must not exceed a critical threshold. The evaporation rate must not be too rapid, allowing sufficient time for the particles to reach the edge of the droplet. Additionally, the Marangoni flow must act in a secondary role relative to the capillary flow.

In the MIX mode, the evolution of the droplet resembles the Stick-Slip (Jumping) mode, with multiple instances of contact line pinning and depinning. Initially, the droplet proceeds through the CCR mode, however, depinning occurs once the contact angle reaches a predefined threshold (minimum value). Then, the droplet returns to the CCR mode until the next depinning occurs. 43, 80, 81 The key difference is that the time intervals between successive depinning events are longer in the Stick-Slip mode, and the minimum contact angle required for depinning is smaller. 82, 83 During the pinning phase, particles accumulate on the contact line and form a ring. Upon de-pinning, another ring is created as the contact line shifts to a new position (**Figure 2c**). Thus, the repeated cycle of pinning and de-pinning phases results in the formation of multiple concentric rings of particles on the substrate. 48, 84

Manipulation of assembly patterns by materials in droplet

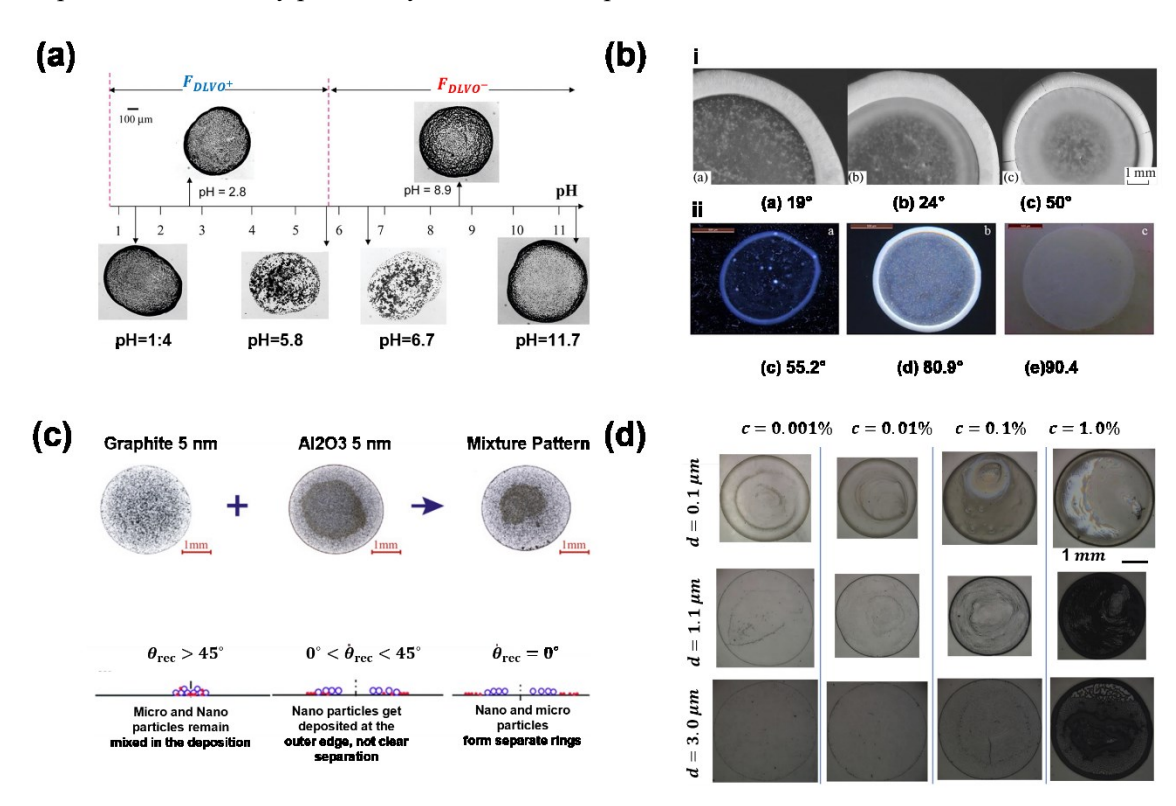


FIGURE 3 Deposition patterns obtained after evaporation of sessile droplets containing different compositions. (a) pH value of the liquid. Adapted with permission. ⁸⁵ Copyright 2010, American Chemical Society. (b) Initial contact angles of the droplet. Reproduced with permission. ⁸⁶ Copyright 2016, Springer Nature. (c) Sessile droplet containing multi-species nanoparticles on different substrate. Reproduced with permission. ⁸⁷ Copyright 2017, Elsevier. (d) Combination of particle size and concentration. Adapted with permission. ⁸⁸ Copyright 2019, Elsevier.

To mitigate the coffee ring effect, numerous studies have documented experiments regarding the pH control of liquids in the literature. It has been demonstrated that the DLVO forces, which are composed of electrostatic and van der Waals forces, influencing the deposition pattern of particles on the substrate are

impacted by the solution's pH. At pH \geq 5.8, there exists an attractive and a repulsive DLVO force, respectively (**Figure 3a**). The fundamental difference between low pH and high pH deposits is that low pH results in particles being attracted close to the substrate, leading to the formation of thick and homogeneous deposits, whereas high pH causes a substantial proportion of particles to not be attracted to the substrate, resulting in nearly all particles being deposited in the peripheral ring. In general, coffee rings are more likely to form when the pH of the solution is over neutral. This is because solutions with a pH higher than neutral have a lower surface tension than acidic or basic solutions. Lower surface tension means that the liquid is less likely to flow back into the center of the droplet after evaporation, resulting in a higher concentration of solutes at the edge of the droplet, which leads to the formation of the coffee ring. 90-92

The initial contact angle determines how well the droplet spreads over the surface. A hydrophobic substrate will cause the droplet to form a more compact shape with a higher contact angle, while a hydrophilic substrate will cause the droplet to spread out more thinly with a lower contact angle. **Figure 3b** illustrates the deposit of particles on various hydrophilic surfaces⁸⁶ (initial contact angle). On substrates with high wettability and smaller contact angles, drying droplets tend to form ring patterns. Conversely, on substrates with lower wettability and larger contact angles, a greater concentration of nanoparticles is observed in the center of the peripheral rings.⁹³ However, it is important to note that the effect of substrate wettability on the coffee ring effect is also dependent on other factors such as the size and concentration of the particles in the droplet, the rate of evaporation, and the surface tension of the liquid.^{94, 95}

Experimental research is done on the effects of multi-species nanoparticles on the deposition patterns from evaporating sessile droplets.^{87, 96} For hydrophobic substrates, the evaporation mode is CCA, and the microparticles and nanoparticles are well mixed in the final deposition. On hydrophilic substrates with a contact angle, $0^{\circ} < \theta_{RCA} < 45^{\circ}$, there are three distinct regions, starting from the outermost part of the droplet and extending towards the center (**Figure 3c**). These regions consist of a nanoparticle-only region, a region of mixing between microparticles and nanoparticles, and an internal region of microparticles only. For hydrophilic substrates with a contact angle θ_{RCA} =0, the nanoparticles are heavily aggregated at the contact line (CL), thus preventing the CL from receding. In this case, the nanoparticles and microparticles are almost completely separated. Multi-species nanoparticles will also influence the near-wall particle motion and evaporation rate.⁹⁷ Take the sessile droplets containing a hybrid of tracer particles and Si/Ag nanoparticles as an example, the tracer particle motion showed a circling pattern at the initial evaporation stage due to non-uniform evaporation rates. The addition of Si/Ag nanoparticles enhanced the droplet evaporation rate and influenced the pinning and depinning of the contact line, resulting in an irregular deposition pattern.

Recent studies have also investigated the coupling effect of the particle size and concentration on deposit formation. For a constant particle size, the ring width increases with concentration and that three distinct deposit types—discontinuous monolayer rings, continuous monolayer rings, and multilayer rings can be

produced through the combination of different particle concentrations and sizes (**Figure 3d**). 88 It has also been observed that, for smaller particle sizes, the particles readily adhere to the contact line and can be tightly packed with each other during evaporation, leading to the formation of ring patterns on substrates with smaller contact angles. 66, 98, 99 On the other hand, larger particle sizes tend to result in the formation of internal deposits or uniform deposit patterns on various substrates. 100

Manipulation of assembly patterns by droplet drying environment

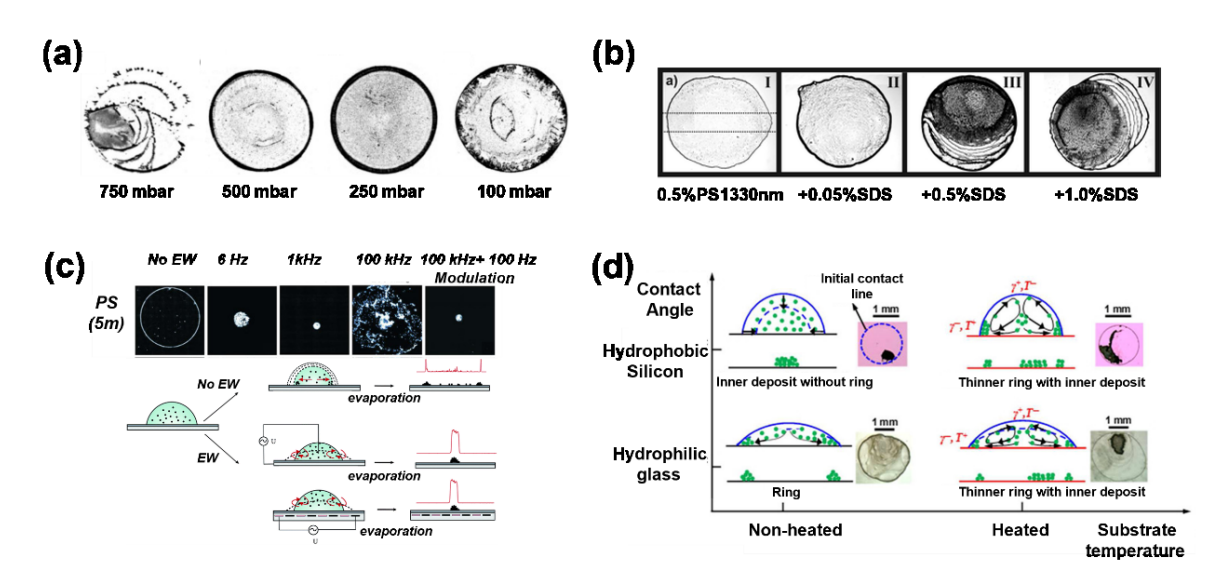


FIGURE 4 Deposition patterns obtained after evaporation of sessile droplets in different drying environments. (a) Ambient pressure. Adapted with permission. Copyright 2012, Elsevier. (b) Surfactants. Adapted with permission. Copyright 2012, American Chemical Society. (c) Electrowetting. Adapted with permission. Copyright 2011, The Royal Society of Chemistry. (d) Combination of substrate temperature and substrate hydrophobicity. Adapted with permission. Society. Copyright 2016, American Chemical Society.

The effective diffusion coefficient of water vapor in the atmosphere increases as the ambient pressure decreases, leading to an increase in the evaporation rate. The evaporation of droplets at different pressures leads to distinct deposition patterns. At 750 mbar, evaporation results in 'stick-slip' behavior, while at 500 mbar, a uniform ring forms. At 250 mbar, a wider ring is produced, while at 100 mbar, a strong outward flow occurs, causing increased particle deposition near the contact line (**Figure 4a**). A slower evaporation rate at low ambient pressure leads to a more pronounced coffee ring effect as the suspended particles have more time to move towards the edge of the droplet. Conversely, a faster evaporation rate at high ambient pressures results in a less pronounced coffee ring effect as the suspended particles do not have enough time to move towards the edge of the droplet. Moreover, the ambient pressure affects the shape of the droplet during evaporation, with low ambient pressures leading to symmetric evaporation resulting in a circular deposit and high ambient pressures causing asymmetric evaporation resulting in an elliptical or irregular deposit. One in temperature deposit and significant properties are also been found when the ambient temperature changes. For example, experiments on water droplet with drying temperature from room to near boiling point temperature (90 °C) demonstrate that

polystyrene nanospheres accumulate at the air-liquid interface rather than at the droplet edge. 107

The addition of surfactants significantly influences the deposition pattern during droplet evaporation. An increase in surfactant concentration results in the creation of a strong Marangoni flow towards the center of the droplet, preventing most of the particles from reaching the contact line and resulting in more uniform particle deposition (**Figure 4b**).⁷⁶ Furthermore, surfactants can reduce the surface tension and alter the contact angle of the droplet, leading to a more uniform spreading and a more homogeneous deposition pattern, with less pronounced coffee ring formation.^{108, 109} Surfactants can also have a destabilizing effect, leading to non-uniform deposition patterns of so-called 'fingers' or 'channels'^{110, 111} particularly for certain types of surfactants, such as ionic surfactants, which can induce electrostatic interactions between the droplet and the substrate.

Electrowetting alters the wetting behavior of a droplet on a substrate by applying an electric field. This technique can reduce the coffee ring effect and lead to more uniform deposition by reducing the concentration gradient caused by differential evaporation rates.^{112, 113} Researchers have found that electrowetting hinders coffee ring formation at low AC frequencies,¹⁰² as the internal flow field generated by electrowetting prevented the accumulation of solutes along the contact line, resulting in a shift from a coffee ring to a dot pattern (**Figure 4c**), but at high frequencies above 100 kHz, the contact line becomes pinned and produces a coffee ring-like pattern due to inertia. In addition to the reduction of the coffee-ring effect, electrowetting can also be used to induce the formation of specific patterns during droplet evaporation by applying a spatially varying electric field,¹¹⁴ leading to the creation of complex structures with potential applications in microfabrication and surface patterning.

Substrate heating has a significant impact on the evaporation dynamics of droplets, which can affect the final deposition pattern. The rate of evaporation at the center of the droplet increases as the temperature of the substrate rises, leading to the formation of Marangoni flow that can reduce the coffee ring effect. However, in some cases, such as on hydrophobic substrates, substrate heating can change the evaporation mode from CCA to CCR, resulting in the formation of ring-shaped deposits. On hydrophilic substrates, heating promotes the formation of thinner rings with internal deposits due to enhanced Marangoni convection at higher substrate temperatures (**Figure 4d**). Heating the substrate is also effective in separating nanoparticles from larger particles at the contact line of a droplet by generating a "strong" Marangoni circulatory flow inside the droplet that can counteract the coffee ring effect and allow for separation based on size. 115

Assembly on a liquid substrate

The utilization of liquid-liquid interfaces as a substrate for the drying of colloidal droplets has recently garnered considerable attention as a promising approach for the creation of organized structures. The capacity to manipulate the interfacial properties of the liquid-liquid interface, such as its surface tension and

wettability, provides control over the arrangement and deposition of colloidal particles on the interface. One key advantage of liquid substrates is their flexibility and deformability, 116, 117 which allows for greater freedom in the assembly and transfer of colloidal particles, thereby reducing the probability of defects and cracks that can occur with solid substrates. Additionally, the liquid-liquid interface can act as a self-healing surface, enabling the removal and repositioning of particles without leaving behind any visible traces. The formation of ordered structures on solid substrates can be impeded by surface defects and impurities, which can act as nucleation sites for defects within the patterns. However, the liquid-liquid interface can effectively serve as a purification mechanism, effectively filtering out any impurities and defects during the assembly process. In addition to the aforementioned advantages, liquid-liquid interfaces offer versatility in terms of the materials that can be deposited and organized at the interface. For instance, particles that are not compatible with solid substrates due to their size, shape, or surface properties can often be easily assembled and transferred on a liquid-liquid interface.

Morphology evolution of droplets on a liquid substrate

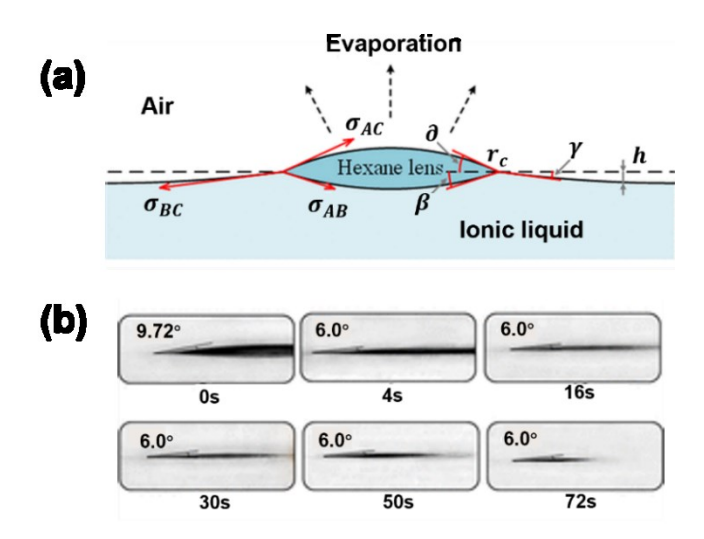


FIGURE 5 Droplet evaporating on another immiscible liquid surface. (a) Schematic diagram of the cross section of a droplet. Adapted with permission.²³ Copyright 2021, American Chemical Society. (b) The side view of the morphology evolution. Reproduced with permission.¹¹⁸ Copyright 2019, American Chemical Society.

A theoretical framework was proposed for predicting the morphological transformation of droplets during evaporation on an immiscible liquid substrate.^{23, 119} The droplet shape is characterized by two spherical crowns (**Figure 5a**). The angles between the upper spherical crown, the lower spherical crown, the liquid substrate surface, and the horizontal plane at the contact line are denoted as α , β , and γ . The interfacial tensions between the droplet and the liquid substrate σ_{AB} , the droplet and the air σ_{AC} , and the liquid substrate and the air σ_{BC} are also considered. In this study, it was deemed appropriate to employ the Neumann triangle equation rather than the Young's equation in analyzing liquid surfaces.²³ In the CCA evaporation mode, droplet evaporation on the surface of the liquid substrate is the dominant scenario. However, a gradual

decline in the contact angle is noted during the later stages of evaporation, along with a contraction of the contact line (**Figure 5b**). Drops spreading on a liquid-fluid interface show similarities to those on a rigid wall during early stages, suggesting interface properties don't play a major role. However, the spreading behavior is logarithmic, resembling coalescence. This raises questions about the role of interface curvature. Low viscosity liquids require attention due to drop shape oscillations before reaching equilibrium.¹¹⁸

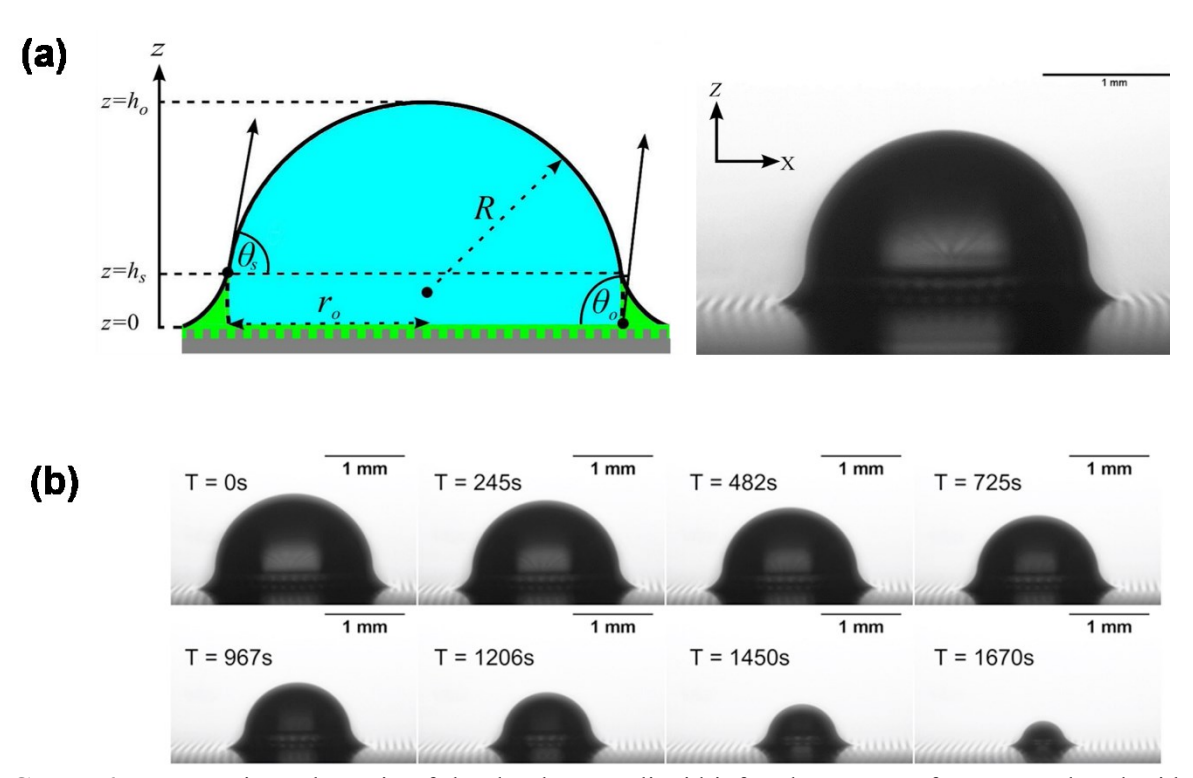


FIGURE 6 Cross section schematic of the droplet on a liquid-infused porous surface. Reproduced with permission. ¹²⁰ Copyright 2015, American Chemical Society. (a) The theoretical model. (b) The side view of the morphology evolution.

Different from a sole liquid substrate, when a solid substrate possesses porosity, the liquid can infiltrate the pores and forms a liquid-infused porous surface, commonly known as SLIPS (Superhydrophobic Liquid-Infused Porous Surfaces). SLIPS represent a distinct form of liquid substrate, distinguished by the presence of an immiscible lubricating liquid infused into the porous surface. Further, wetting ridges will be formed at the edge of droplet, different from a spherical crown that is observed in droplet on a solid substrate as shown in Figure 6a. More important, the resultant balance between the three interfacial tensions at the contact line between the droplet, the lubricating liquid and the air can be well described by the Neumann force triangle that are used to describe the droplet on a liquid substrate. This type of surface was found to support high apparent contact angles (~100°) for droplets and exhibit high mobility at the apparent contact line, enabling evaporation in the CCA mode (Figure 6b). The lubricating liquid creates a low-energy interface that is responsible for the unique properties of the surface, including its repellent behavior towards various substances. The presence of the lubricating liquid on the surface also enables evaporation in the

Cassie-Baxter mode, which enhances the efficiency of heat transfer and reduces the formation of bubbles or hot spots.^{121, 122} This makes SLIPS a promising material for use in cooling systems, such as in power plants or electronic devices¹²³.

Assembly patterns after complete drying on a liquid substrate

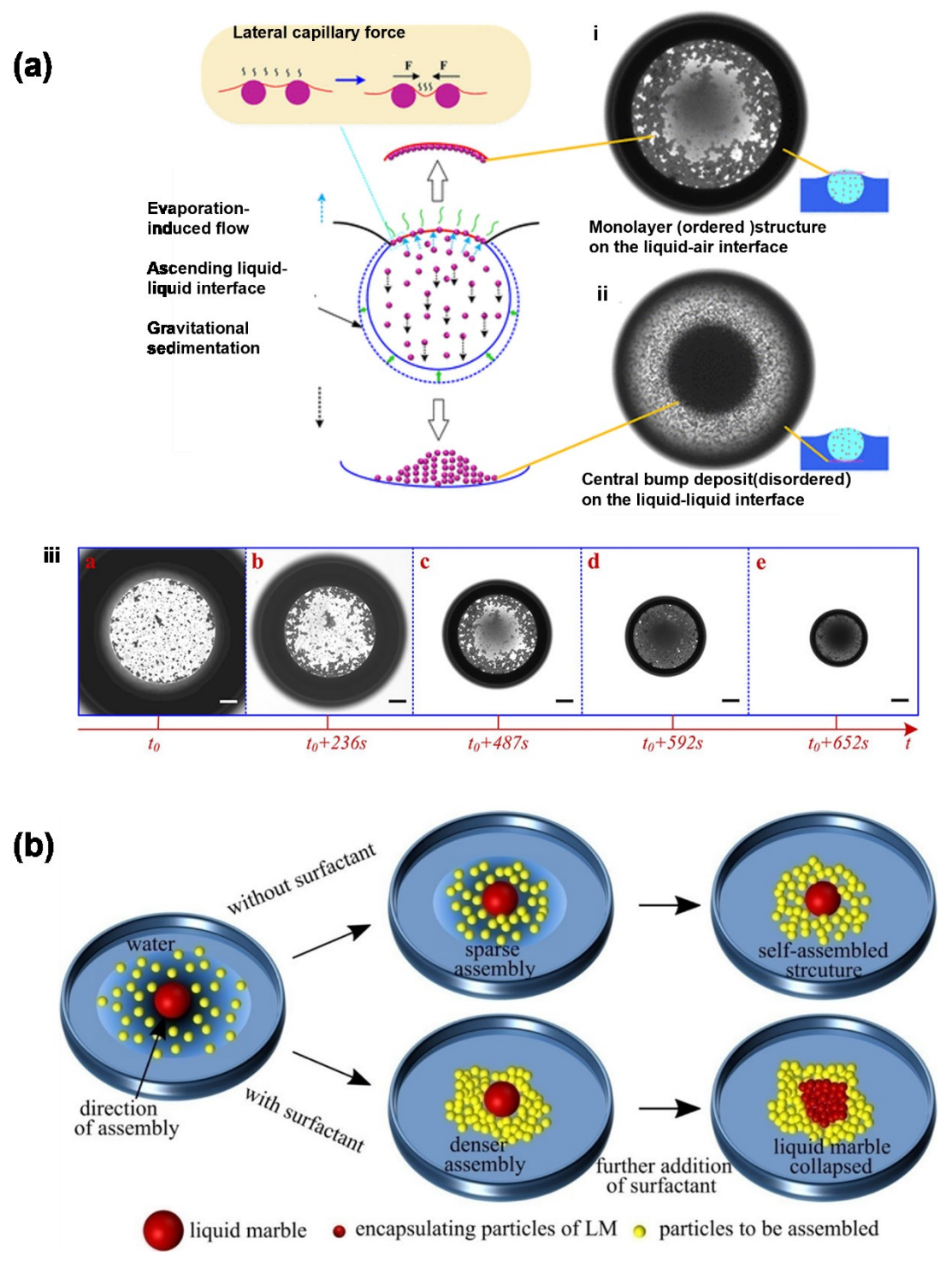


FIGURE 7 Assembly of particles on liquid substrates. (a) The theoretical model and the top view of the self-assembly of particles at the liquid—air interface as the droplet evaporates. Reproduced with permission. ¹²⁴

Copyright 2019, American Chemical Society. (b) The collapse of liquid marbles (LMs) and LM-mediated assembly by controlling the surface tension of the liquid substrate. Adapted with permission. ¹²⁵ Copyright 2019, American Chemical Society.

An ordered particulate monolayers is created through the evaporation of colloidal droplets situated at the liquid-air interface on liquid substrates and the deposition of central bumps at the liquid-liquid interface.¹²⁴ At the liquid-air interface, there were individual particles and small islands sparsely scattered. With the ongoing process of evaporation, these particles began to aggregate, and the islands expanded in size. Eventually, a single layer structure formed at the liquid-air interface (Figure 7a, i). The central bump deposition of disordered particles at the liquid-liquid interface was noted to arise from the rapid convergence of descending particles and the ascending liquid-liquid interface (Figure 7a, ii & iii). The formation of ordered structures is attributed to evaporative convection and capillary forces, which were able to assemble the patterns into monolayer formations at the liquid-gas interface as a result of weak capillary flow and triple line contraction. The liquid substrate plays a crucial role in this drying process, as the properties of the liquid substrate, such as its surface tension and wettability, can influence the final structure and ordering of the particles in the monolayer. 126 The role of surface tension is also critical in the collapse of multilayered liquid marbles (LMs). 125 The surface tension required for collapse depended on the volume of the LMs, with larger LMs being less stable and requiring a higher surface tension for collapse. The collapse occurred when the surface tension force approached the weight of the LM, as determined through force analysis. As shown in figure 7b, the addition of surfactants decreases the surface tension of the liquid substrate on which the particles were placed resulted in a steeper meniscus shape and stronger capillary forces, leading to a denser assembled structure. The release of the core liquid of the LM during collapse and the resulting Marangoni flow also contributed to the denser assembly.

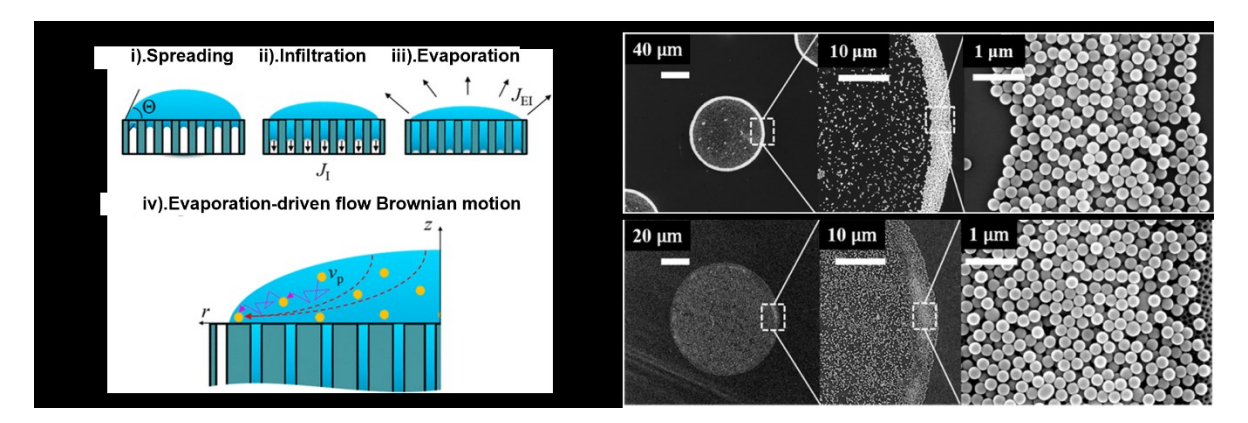


FIGURE 8 Droplet drying on a porous liquid-infused substrate. Reproduced with permission. ¹²⁷ Copyright 2015, American Chemical Society. (a) The three stages of drop deposition (i, ii and iii) and particle motion (iv). (b) Comparison of deposition on glass without pores (upper panel) and on nanoporous anodic aluminum oxide (AAO) substrates with a pore diameter of 55 nm (lower panel)

The deposition process of colloidal droplets on a porous substrate was found to consist of three stages 127:

spreading, infiltration, and evaporation (**Figure 8a**). The deposition was determined by the interaction between particle motion, solvent evaporation, and permeation. When the solvent could be completely absorbed by the porous substrate, the competition between particle motion towards the contact line and solvent permeability was crucial in determining the final deposition morphology. The coffee-ring effect is not observed on nonporous glass substrates unlike the porous AAO substrate, which suggests that an increase in porosity can prevent the coffee-ring effect (**Figure 8b**). Further, if the time required for the particles to form the first layer of coffee rings was longer than the time required for complete solvent permeation, then solvent permeation dominated, and the coffee ring effect was suppressed. Conversely, if the time required for the particles to form the first layer was shorter than the time required for complete solvent permeation, particle deposition dominated and coffee ring deposition was formed. The influence of substrate pore size on the extent of capillary-driven coffee ring effect is investigated. The results indicate that a decrease in pore size is associated with a reduction in the observed coffee ring as a result of the slower capillary flow. On the other hand, when the pore size is excessively large, the nanoparticles become absorbed into the substrate along with the draining solute, resulting in a lack of particle deposition.

Assembly in a suspended air environment

The evaporation of droplets suspended in air can bypass solid surfaces and boundary effects, and a fully suspended air-water interface provides the necessary conditions for fabricating freestanding nanocomponents. In the process of droplet drying in a fully suspended air environment, the morphology of the dried materials is especially influenced by the competition between the diffusion of dispersed material in solution and the rate of solvent evaporation. ^{129, 130} This section will examine the evaporation of air-suspension droplets containing colloidal particles, 2D materials, and 1D materials (nanotubes).

Assembly of rigid particles

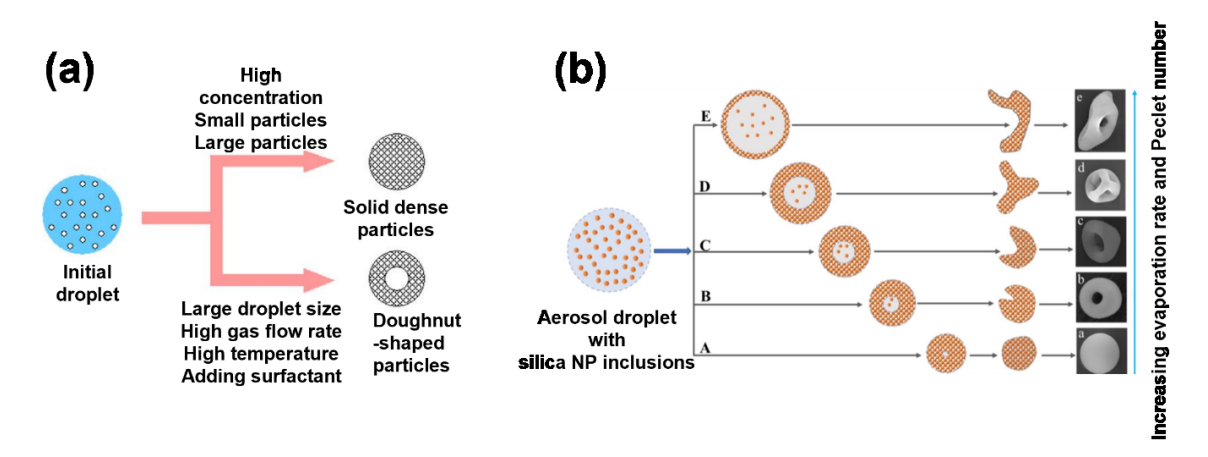


FIGURE 9 Assembly of rigid particles by spray drying (a) Morphology changes with the particle size, the droplet size, the viscosity of droplet, the drying temperature, the gas flow rate, and the addition of surfactant. Adapted with permission.¹³¹ Copyright 2003, Elsevier. (b) Schematic of the drying process at different Péclet

numbers and the resulting predicted morphologies of the final dried silica microparticles. Adapted with permission.³³ Copyright 2020, American Chemical Society.

Droplet size, temperature, and surfactant addition are some of the parameters that can be controlled to produce different rigid particle shapes and sizes. 131, 132 For example, small droplets with large and small solid particles produced spherical particles, while toroid particles were produced with larger droplets, high temperature, high gas flow rate, and surfactant addition (Figure 9a). Another important factor that affects the morphology of dried particles is the Péclet number, which is the ratio of the evaporation rate to the diffusion coefficient.³³ For instance, at a low Péclet number (below 23.8), the dried silica particles were spherical with a smooth surface due to a slow drying process allowing for inclusions to redistribute through diffusion. However, as the Péclet number increased, the surface of the particles showed pits, hollows, crinkles, and doughnut shapes due to the flexural process triggered by the solute-to-gel transition. This process caused the shells to become unable to withstand the pressure of the later stages of the drying process, resulting in the unique shapes and textures (Figure 9b). In addition to the factors mentioned above, the viscosity of the droplets also plays a critical role in determining the morphology of the dried particles. High viscosity droplets tend to produce more irregular shapes due to their slower evaporation rate, leading to the formation of non-spherical particles with pits and crinkles. On the other hand, low viscosity droplets tend to produce smoother and more spherical particles due to their faster evaporation rate, which allows the droplet to maintain its shape during the drying process^{133, 134}.

The fabrication of freestanding nanocomponents using acoustic levitation self-assembly of nanoparticles is an innovative technique that allows for the precise control of particle morphology and structure¹³⁵. The fabrication process involves casting a concentrated suspension of PS-Au NCs into droplets on the surface of suspended water. The droplet shrinks vertically but remains unchanged horizontally, forming a double-layered building block (**Figure 10a**). A suspension of DNA-NSs is introduced into the droplet, forming a three-layer nanoassembly after drying (**Figure 10b**). Lastly, a three-dimensional hollow scaffold structure is formed by introducing CTAC solution along with DNA-NSs and adding a chloroform solution of PS-Au NCs at the bubble-water boundary. The resulting structure is composed of a network of hollow tubes with the DNA-NSs in the middle layer acting as a scaffold (**Figure 10c**). Similar to the spray drying method, the morphology and structure of the particles formed through this method can be also controlled by adjusting the concentration of the nanoparticle suspension, the type of solvent used, and the evaporation rate of the solvent. ^{136, 137} For instance, increasing the concentration of the nanoparticle suspension can lead to the formation of larger and more irregular particles structures.

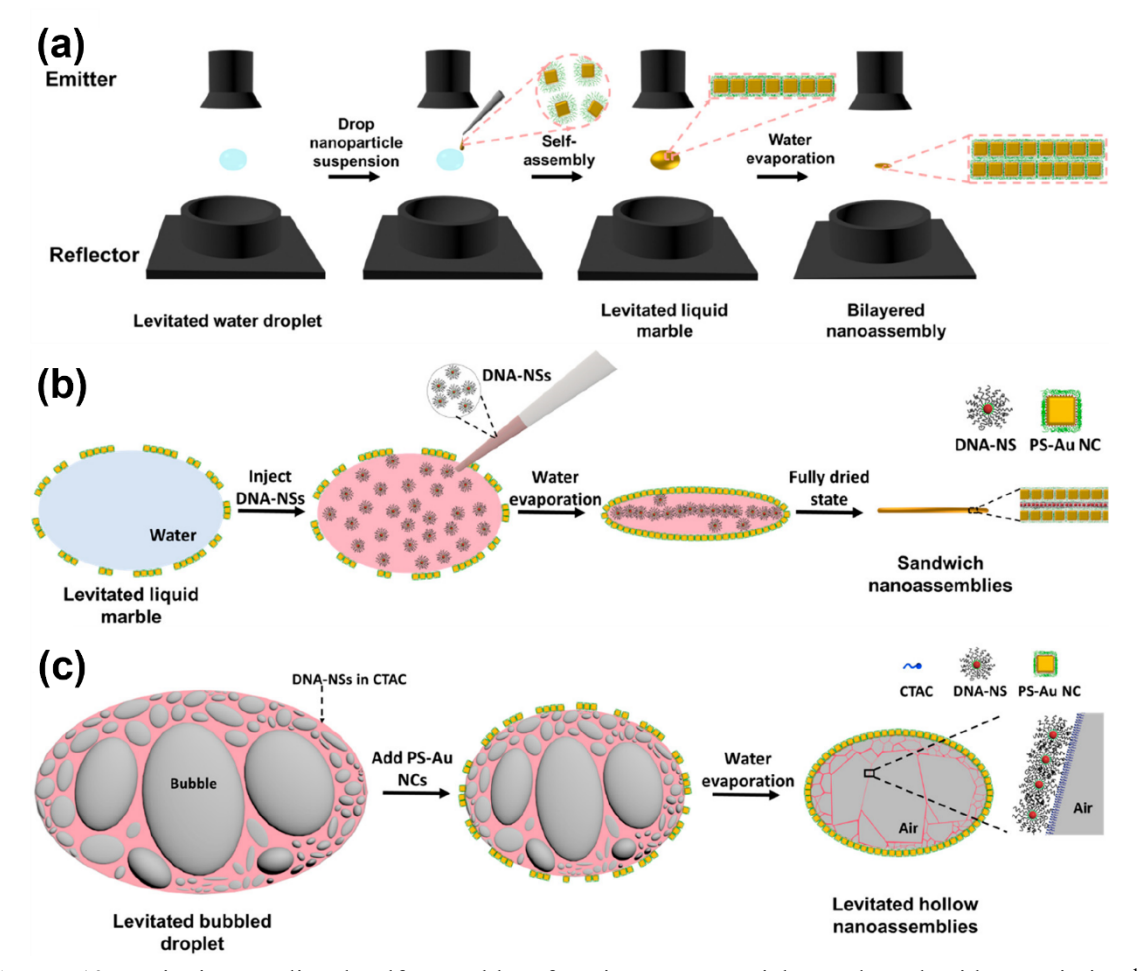


FIGURE 10 Levitation mediated self-assembly of various nanoparticles. Adapted with permission. ¹³⁵ Copyright 2019, American Chemical Society. (a) The assembly of a bilayer nanoassembly. (b) Assemble sandwich nano-assemblies by injecting a concentrated suspension of DNA-NSs. (c) A levitated DNA-NSs droplet with bubbles.

Assembly of mechanical deformable nanomaterials

In contrast to colloidal particles, which generally do not experience mechanical deformation during solution evaporation, 1D and 2D nanomaterials are highly susceptible to deformation, folding, and stacking due to compression. The dispersion of these materials in liquid solutions also differ, with 2D materials tending to migrate towards the liquid-air interface while 1D materials remain in the droplet. During early stages of evaporation, graphene sheets tend to aggregate at the liquid-gas interface while carbon nanotubes remain within the droplet, with only a small fraction penetrating the droplet surface and being exposed to air. As evaporation continues, the graphene sheets crumple and assemble at the liquid surface while carbon nanotubes within the droplet deform and accumulate, resulting in crumpled graphene-assembled nanoparticles after complete evaporation of the encapsulated carbon nanotubes. A theoretical model was proposed to systematically characterize the wrinkling and self-assembly of two-dimensional materials.³⁶ The model incorporates a rotating spring to describe the deformation of 2D sheets and a mechanical slider to model the bonding energy between a single 2D sheet or adjacent sheets during self-folding or overlap

(**Figure 11a, i**). This model offers valuable insight into the behavior of 2D materials during self-assembly and can provide a foundation for the development of advanced materials with tailored properties. The findings indicate that, at low evaporation pressure and small total graphene sheet area, self-folding of single sheets is minimal and assembly dominates, whereas at high evaporation pressure and large total graphene sheet area, both folding and assembly occur concurrently. Furthermore, another energy-based model was proposed to examine the migration, crumpling, and assembly mechanisms of carbon nanotubes and graphene suspended in liquid droplets during solution evaporation(**Figure 11a, ii & iii**).³⁷ This model can predict the wrinkled morphologies of the composite particles resulting from varying graphene mass fractions and CNT diameters.

Experimentally, a one-step aerosol method was utilized to assemble carbon nanotubes and graphene into hybrid nanospheres (CGHN).¹³⁸ This aerosol-assisted assembly method prevents the formation of CNT bundles and restacking of individual graphene sheets, effectively increasing the specific surface area (**Figure 11b**). The CGHNs are highly stable due to strong π – π interaction and can form efficient charge transfer pathways with improved electronic conductivity, resulting in superior oxygen reduction reaction performance to commercial Pt/C catalyst after nitrogen and phosphorus doping. In a similar experiment, isotropic compression of graphene oxide sheets to form a near-spherical particle has been achieved through aerosol-assisted capillary compression.¹³⁹ The concentration of GO in aerosol droplets can affect the size and degree of crumpling of particles. Higher concentrations of GO result in larger particles with fewer ridges and vertices, while lower concentrations lead to smaller particles with more crumpling (**Figure 11c**). Thicker GO flakes with higher bending modulus from higher GO concentrations make the particles stiffer against deformation, resulting in less crumpling and larger particles.

The above experiments highlight the use of aerosol methods in the assembly of nanomaterials, specifically carbon nanotubes and graphene. The aerosol method has the advantage of providing a suspended air environment for the assembly process, which can lead to more controlled particle formation compared to other techniques. For example, TiO2 hierarchical hollow microspheres with improved photocatalytic performance were made using an ultrasound-assisted aerosol-spray method followed by topotactic transformations. The microspheres were assembled from TiO2 mesocrystal nanosheets, and their unique structure allows for efficient light absorption, fast charge separation, and improved mass transport. ¹⁴⁰ An efficient method has been developed to synthesize 2D layered WS2 nanosheets assembled on 1D WS2 nanostructures for the ultrasensitive detection of NO2. ¹⁴¹ Researchers combined the aerosol-assisted chemical vapor deposition (AA-CVD) method with H2-free atmospheric pressure CVD, enabling direct integration of the sensing material onto the sensor transducer with high growth yield and uniform coverage. This has significant implications for the development of advanced sensing materials and detecting harmful gases.

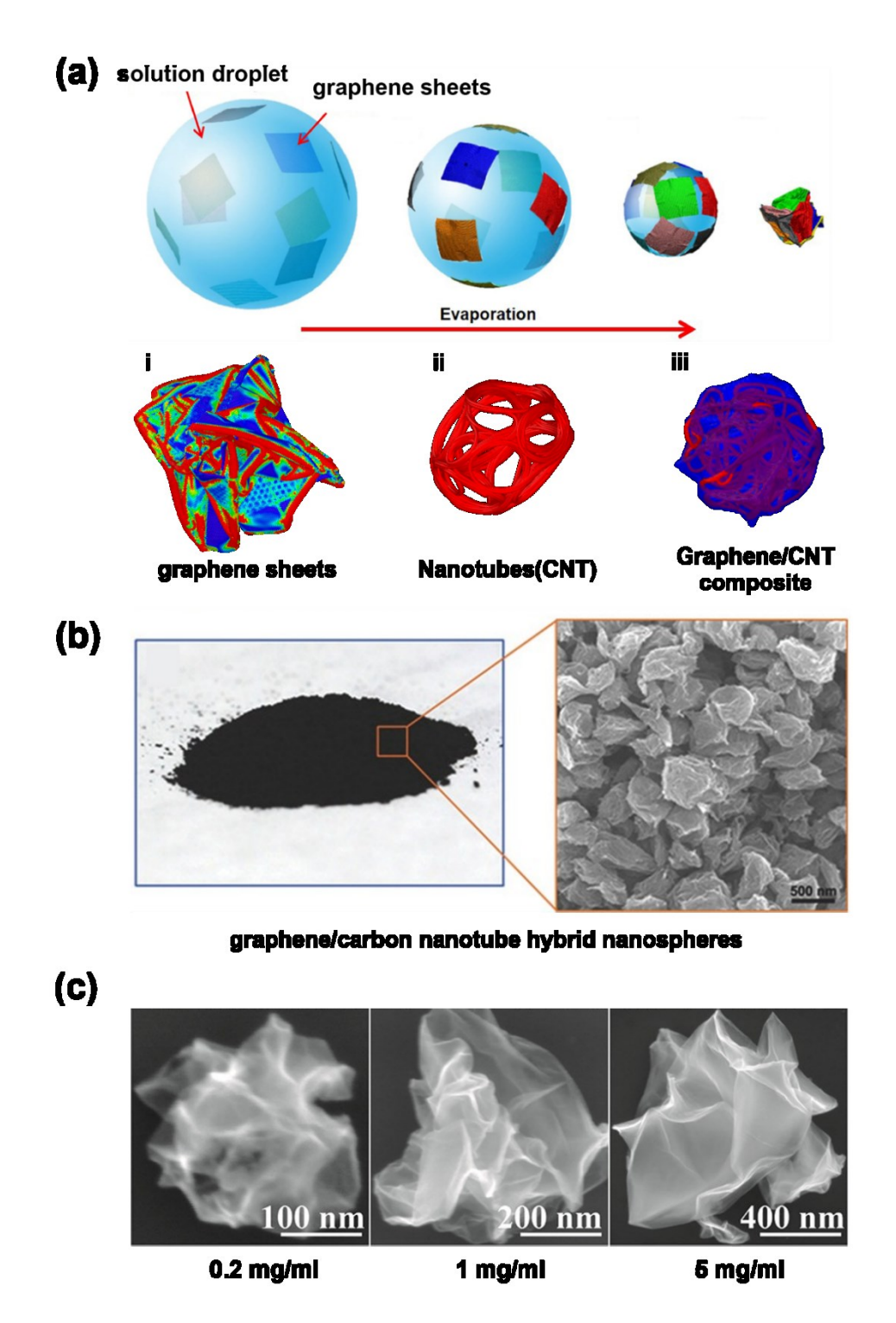


FIGURE 11 The crumbled structures obtained by assembling 2D/1D materials. (a) Schematic illustration of assembly process of mechanical deformable 2D sheets by droplet drying in a air and snapshots of simulated assembly patterns of graphene sheets(i), nanotubes(ii), and mixture(iii) after complete evaporation of liquid. Reproduced with permission.³⁷ Copyright 2020, American Chemical Society. (b) Experiments of drying droplets containing nanotubes and graphene into hybrid nanospheres (CGHNs). Reproduced with permission.¹³⁸ Copyright 2016, John Wiley & Sons. (c) Particles of crumpled GO sheets by evaporating aerosol droplets at different concentrations. Adapted with permission.¹³⁹ Copyright 2011, American Chemical Society.

Applications in ink-based printing technologies

Ink-based printing technology has come a long way since the days of the Gutenberg press, where movable type was used to create printed pages. Today, modern inkjet printers can produce high-quality images and text with incredible speed and precision. One of the key innovations that have driven this progress is the ability to control the way ink droplets dry on paper. In this section, we will explore how the principles of colloidal droplet drying have been embodied in applications to ink-based printing technology.

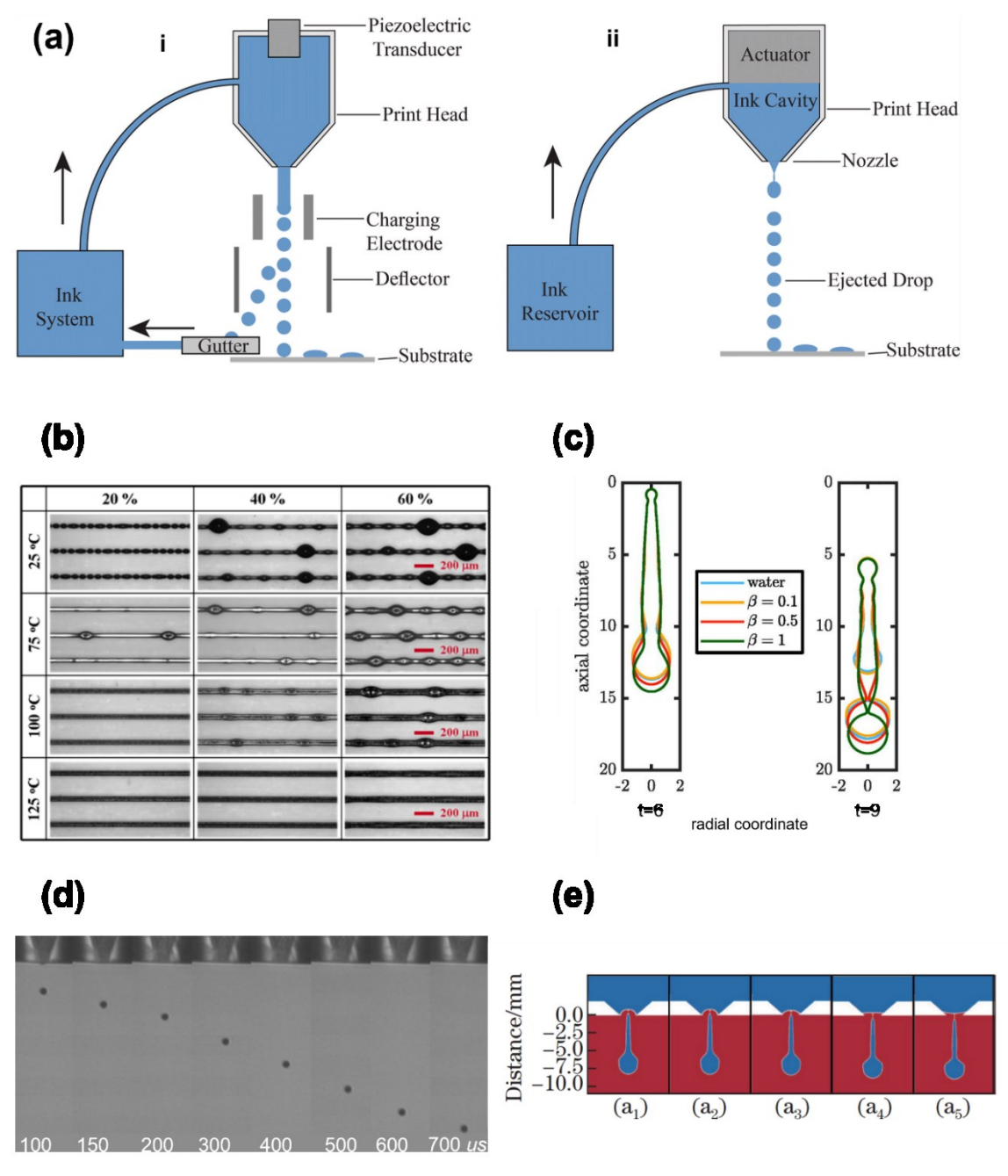


FIGURE 12 Ink-based printing technologies. (a) Schematic diagram of two types of inkjet printing systems: (i) continuous inkjet printer and (ii) drop-on-demand printer. Adapted with permission. ¹⁴² Copyright 2020, Springer Nature (b) inkjet-printed lines with 200 Hz printing frequency for various droplet overlaps and substrate temperatures (continuous inkjet printer). Adapted with permission. ¹⁴³ Copyright 2018, MDPI. (c)

droplet shape for different surfactant strengths after pinch-off from the nozzle (drop-on-demand printer). Reproduced with permission. ¹⁴⁴ Copyright 2021, AIP. (d) The conditions of droplet formation and injection for the Ag nanopowder suspension with pulse voltage of ±33 V. Reproduced with permission. ¹⁴⁵ Copyright 2008, IOP Publishing. (e) Time sequence of ink droplet at breakup at different nozzle inner wall contact angle. Reproduced with permission. ¹⁴⁶ Copyright 2019, Springer Nature.

Inkjet printing systems can be classified into two types: continuous inkjet (CIJ) and drop-on-demand (DoD). The former employs a piezoelectric transducer to break up ink into droplets (**Figure 12a, i**), whereas the latter ejects single droplets using an actuator (**Figure 12a, ii**). CIJ technology is suitable for high-speed printing applications such as labeling, packaging, and coding, thanks to its high-resolution printing capabilities. The small diameter of the ink droplets (10-100 microns) facilitates high-resolution printing, making it versatile across various substrates like plastic, metal, glass, and paper. A recent study has shown that low-temperature adhesive bonding using continuous inkjet printing can be employed to bond fragile M(O)EMS devices, thus mitigating bonding-induced defects and enhancing device reliability. Drop-on-Demand (DoD) technology is ideal for printing on materials such as textiles and ceramics, where precision and droplet control are critical.¹⁴⁷ DoD technology allows for customization of droplet size by manipulating the voltage applied to the piezoelectric crystal or by adjusting the temperature of the thermal printhead, making it suitable for high-precision printing tasks.¹⁴² Additionally, DoD technology is well-suited for printing on irregular or non-flat surfaces.

The principles of colloidal droplet drying have been integrated into inkjet printing in various ways to control ink droplet drying behavior and achieve high-quality prints. One approach is to modify the substrate by applying a pre-treatment, such as heating or plasma, that alters the droplets' interaction with the surface, resulting in smoother and more uniform prints. As the temperature increases, ink droplets solidify faster than the printing period, resulting in a distinct round edge on the substrate. Temperature control is crucial for optimal printing outcomes, 143 and findings from a recent study indicate that the appearance frequency of bulges decreases with temperature increase due to rapid solvent evaporation (Figure 12b). Another approach is to modify the ink itself by adding additives, such as surfactants, that control the surface tension and viscosity of the ink, promoting optimal droplet spreading and merging on the substrate (Figure 12c). 144 The pulse voltage can also have an effect on inkjet printing. 145 A higher driving pulse voltage was needed for the silver suspension to form droplets, with a thinner and longer liquid column and longer pinch-off time. However, the characteristic adjustment time for droplet recombination was shorter than for deionized water. The minimum pulse voltage for ejecting the silver suspension at 30 wt% was ± 33 V (Figure 12d). Below this, droplets couldn't be formed or ejected, and the liquid column broke up below the nozzle and quickly formed a spherical shape. Another study examined how the contact angle of the interior surface affects the optimal contracting angle. ¹⁴⁶ The nozzle inner wall contact angle from a_1 to a_5 are 10°, 50°, 90°, 130° and 170° respectively (Figure 12e). A super hydrophilic surface produced thicker ligaments and higher droplet speed, while a super hydrophobic surface resulted in a thinner and longer tail ligament, potentially reducing

printing quality. A super hydrophilic inner surface was found to be more beneficial for printing quality and throughput rates. Organic and volatile solvents can also be used to control the ink's properties, including viscosity, surface tension, stability, particle size, density, contact angle, leveling performance, and evaporation rate. Advanced droplet ejection technologies like thermal inkjet, be piezoelectric inkjet, sand electrohydrodynamic (EHD) printing enable ink droplets to land on the substrate with high precision and accuracy, resulting in sharp and crisp prints. Finally, controlling the environment in which inkjet printing takes place, such as using heated platens or drying chambers, is crucial for optimal drying times and producing high-quality prints. Overall, the principles of colloidal droplet drying have been embodied in inkjet printing technology to achieve greater precision, speed, and quality in printing. By understanding and controlling the complex physical and chemical factors that govern the drying behavior of ink droplets, researchers and engineers have been able to develop new techniques that enable more efficient inkjet printing.

Applications in the printing of sensors

Inkjet printing has revolutionized the way electronic sensors are fabricated and has become a popular technique in the field of printed electronics. As a non-contact, digital printing process, inkjet printing allows precise placement of small droplets of functional materials on a variety of substrates, including flexible and rigid materials, at high speed and low cost, and has various areas of application ranging from electronic sensors to biomedical applications.

Electronic sensors for anti-counterfeiting

Charged droplets have emerged as a promising tool for the precise printing of complex nanometer-scale patterns with minimal material transfer across different surfaces, facilitated by the voltage differentials between the inkjet and grounded substrate. 155 Various inks were used during the printing process: Suspensions of Ag nanoparticles (Figure 13a, i), Ag nanowires in (Figure 13a, ii), and Ag nanotubes (Figure 13a, iii). The peaks are reported to be approximately 150 nm in thickness and ~ 0.25 V in electric potential. Inkjet printing has also been used as a cost-effective means of flexible electronic sensors, as multi-parameter sensors capable of temperature, humidity, and strain measurements have been produced using silver nanoparticle ink and PEDOT: PSS. 156 (Figure 13b). The demand for stronger anti-counterfeit patterns grows with the advancement of modern materials and printing technology. Photonic crystals exhibit characteristics that allow them to alter light frequency and intensity, making them the ideal materials for printing anticounterfeit patterns. 157-159 Utilizing inkjet-printing, The mono-layered, self-assembled photonic-crystal (SAPCs) patterns were produced on various substrates: 160 Glass (Figure 13c, i), Si wafer (Figure 13c, ii), PP (Figure 13c, iii), and PDMS (Figure 13c, iv). Under daylight conditions the patterns become covert, while under illuminations the patterns display colorful holograms. Additionally, patterned fluorescent arrays of Perovskite materials have been produced¹⁶¹ via an in Situ crystallization process utilizing inkjet-printing as well (Figure 13d). This technology can be used in applications such as anti-counterfeiting labeling.

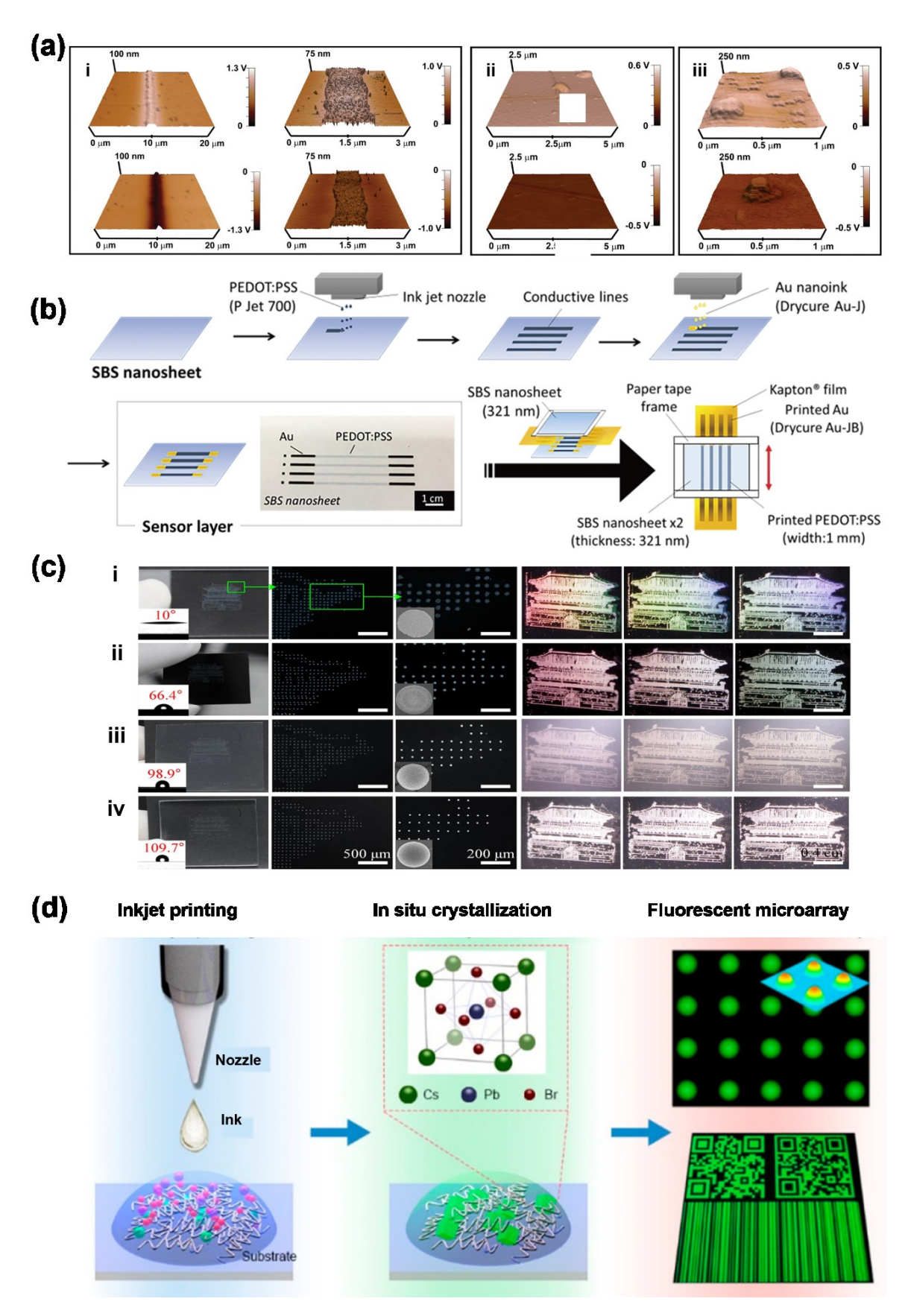


Figure 13 Flexible electronic sensors. (a) 3D KFM images of the samples printed with electrically charged droplet jets utilizing various inks. Reproduced with permission. ¹⁵⁵ Copyright 2010, American Chemical

Society. (b) Droplet spacing of multi-nozzle inkjet printing. Reproduced with permission. ¹⁵⁶ Copyright 2012, American Chemical Society. (c) Photonic crystal printing, self-assembly, and patterning. Reproduced with permission. ¹⁶⁰ Copyright 2016, Springer Nature. (d) Production of patterned fluorescent arrays composed of Perovskite materials via in Situ crystallization. Reproduced with permission. ¹⁶¹ Copyright 2019, American Chemical Society.

Apart from its traditional applications, inkjet printing has emerged as a powerful tool in producing flexible organic electronics. The electronics under discussion consist of thin films of organic materials, specifically polymers and small molecules. ^{162, 163} These materials exhibit distinctive characteristics, including flexibility, low cost, and ease of fabrication, which render them highly promising for the transformation of the electronics industry. Inkjet printing's main advantage lies in its ability to print multiple materials in one go, which is crucial in the fabrication of multi-layer electronic devices. To achieve this, various print heads can be utilized to deposit different materials, including conductive inks, insulating inks, and functional materials, onto the substrate. Furthermore, inkjet printing allows for the accurate deposition of materials with the required thickness and pattern, an essential feature in the production of high-sensitivity and high-selectivity sensors.

Biomedical sensors for healthcare

Biomedical sensors play a crucial role in the monitoring and diagnosis of various medical conditions, and the development of inkjet printing technology has enabled the fabrication of sensors that are highly accurate, reliable, and cost-effective. Inkjet printing technology has been used to fabricate a variety of biomedical sensors, including glucose sensors and pH sensors. These sensors are critical in the monitoring and diagnosis of various medical conditions, including diabetes, cancer, and cardiovascular disease.

Utilizing printed inkjet droplets with the evaporation-induced spontaneous flow on photonic crystal basilica can increase the detection limit for optofluidic analysis from the traditional pipette-dispensed surface-enhanced Raman scattering (SERS) method (**Figure 14a**)¹⁶⁴. The bioaccumulation resulting from the evaporation-induced flow substantially increased the sensitivity of the SERS for optofluidic analysis by a factor of 10⁶ to 10⁷. Microfluids have also been used in the array-based single-cell reverse transcription quantitative PCR (RT-qPCR) assay method for cellular genetic analysis (**Figure 14b**).¹⁶⁵ Droplets containing cell suspension are deposited on the hydrophilic spots of the silicon underneath a layer of cover oil in an array, and after cell counting and thermal lysing, reverse transcription (RT) mix is injected into the droplets to convert RNA to cDNA, then PCR mix is added to the droplets before real-time fluorescence PCR is conducted for genetic analysis. Such sensitive methods have potential applications in rare cell and transcriptional analysis.

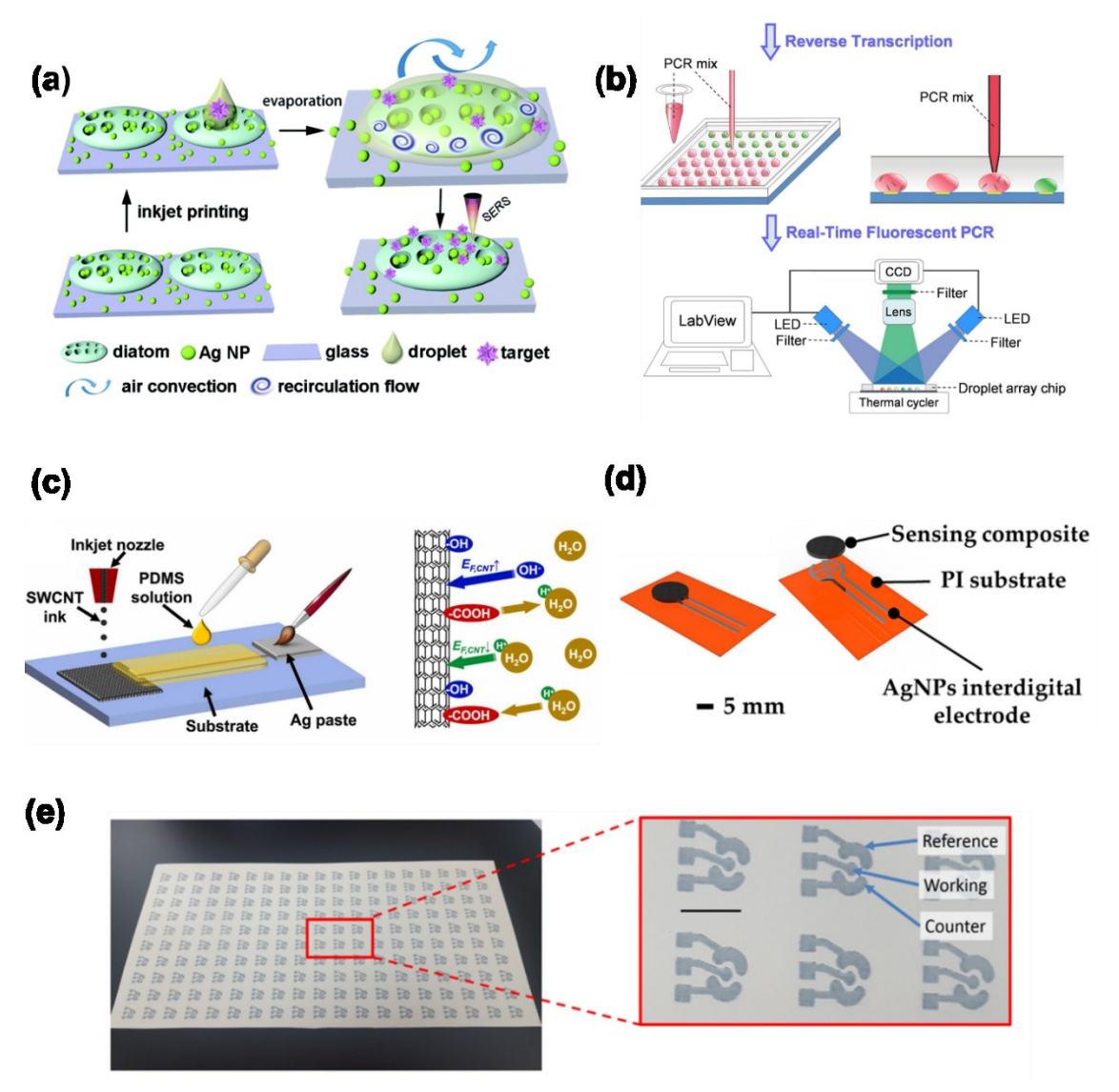


Figure 14 Flexible biomedical sensors. (a) Sub-nanoliter liquid droplets inkjet-printing on photonic crystal basilica. Reproduced with permission. ¹⁶⁴ Copyright 2016, The Royal Society of Chemistry. (b) Droplet array system for single cell gene expression analysis. Reproduced with permission. ¹⁶⁵ Copyright 2015, Springer Nature. (c) Schematic of the fabrication process of a SWCNT-based pH sensing electrode. Reproduced with permission. ¹⁶⁶ Copyright 2016, Elsevier. (d) Schematic illustration of a pressure monitoring sensing unit. Reproduced with permission. ¹⁶⁷ Copyright 2019, MDPI. (e) Photograph of glucose biosensors inkjet-printed on paper with a loop on the device geometry/configuration. Reproduced with permission. ¹⁶⁸ Copyright 2018, Springer Nature.

A method has been developed for depositing functionalized single-wall carbon nanotubes using inkjet printing, which can serve as both electron conduction and pH-sensitive layers. ¹⁶⁶ The mechanism for pH sensing involves doping and de-doping of the carbon nanotubes by hydronium and hydroxide ions (**Figure 14c**). To enhance electron conduction and pH sensitivity, multi-pass printing was utilized to deposit tightly packed thin films and lower electrode resistance. Another area where inkjet printing technology has shown promise is in the development of wearable biomedical sensors. Inkjet printing technology allows for the printing of sensors directly onto flexible and stretchable substrates, which can conform to the contours of

the body. A conductive rubber with surface processing was designed to create a pressure-sensitive insole for real-time planar pressure monitoring. The sensor displayed stable contact resistance, easy manufacturing, and high mechanical durability (**Figure 14d**). Experiments demonstrated its ease of assembly and good sensing performance with inkjet-printed electrodes and a flexible substrate. One novel analytical tool that enables the measurement of physiologically relevant glucose concentrations in human saliva through enzymatic electrochemical detection is presented. This study utilizes inkjet-printing technology to deposit all the necessary components of the glucose sensor onto commercially available paper substrates in a rapid and cost-effective manner (**Figure 14e**). This disposable device includes both electronics and biorecognition elements, making it an efficient and comprehensive solution for glucose monitoring.

Biosensors are critical in the diagnosis and monitoring of various medical conditions, including infectious diseases, cancer, and autoimmune disorders. Inkjet printing technology has become an increasingly popular method for the fabrication of biomedical sensors due to its numerous advantages over traditional manufacturing methods, such as allowing for the deposition of specific biomolecules onto the sensor substrate, enabling the development of highly sensitive and specific biosensors. Inkjet printing technology has enabled the fabrication of microfluidic channels and reaction chambers directly onto the diagnostic device substrate. This allows for the integration of multiple steps in the diagnostic process, including sample preparation, detection, and analysis, into a single device. Inkjet printing technology has also been used to fabricate biosensors that can detect specific biomolecules, such as proteins or nucleic acids, in a sample. The

Conclusion and outlook

This literature reviewed the evaporation of droplets containing colloidal particles, 1D materials, and 2D materials on solid substrates, on liquid substrates, and suspended in air, from mechanics theories to applications. The final dried products depend on a variety of factors, which basically come from the external environment (e.g., temperature, pressure), the base droplet (e.g., wettability, Ph) and the solute (e.g., size, concentration). Despite the considerable research efforts dedicated to this field in recent decades, several challenges remain to be tackled to fully leverage the potential of this approach. The random motion of particles in the droplet can result in non-uniform packing and clustering, leading to the formation of undesired structures.⁸ There is still room for improvement in these strategies such as controlling the droplet evaporation rate, applying external fields, or using surfactants to stabilize the particle dispersion. For 1D materials such as nanowires, the challenge lies in controlling their orientation and alignment within the droplet.¹⁷² In the case of 2D materials such as graphene or MoS2, the challenge is to achieve controlled stacking and interlayer spacing within the droplets.^{173, 174} Methods such as layer-by-layer assembly or chemical vapor deposition can be used to achieve these goals, but needs a careful tuning of the growth parameters.

Looking forward, despite facing challenges, droplet drying-assisted assembly of materials offers emerging opportunities for further exploration. For example, printing nanomaterials-based electronics and biomedicine often requires materials assembly with complex structures, that help promote the interactions of devices with surroundings. Developing new strategies of droplet evaporation that could control the materials assembly with three-dimensional structures or hierarchical assemblies is considered to provide a facile solution. The integration of droplet evaporation with microfluidic systems also represents a promising area of worthy exploration. This integration is expected to achieve a precise control to both geometric morphology and material composition of droplet, thereby significantly benefiting the sensitivity and selectivity for nextgeneration microfluidics-based sensors and actuators. For another example, with the emerging of new 2D nanomaterials and soft materials whose structural features, physical, mechanical, and chemical properties are significantly different with bulk counterparts, assembly them with desirable structures via droplet drying may lead to new mechanics and assembly theory. Besides, the flow field may in turn affect both mechanical deformation and assembly process of materials, and development of theoretical models and simulation approaches that could reflect their dynamic coupling mechanisms will advance fundamental science of materials assembly by droplet drying. In parallel, exploration of new experimental measurement techniques that allow to uncover in situ dynamic mechanical deformation and assembly process during droplet drying is of critical importance, and certainly techniques that help measure full three-dimensional flow fields of liquid in droplet will also be highly needed in the future. Last but not the least, droplet drying based manufacturing or printing large-scale functional structures usually needs a continuous, uninterrupted layerby-layer or line-by-line material assembly with seamless integration (sometimes desirable assembly interfaces/boundaries for multiple materials), where the individual droplet spreading, coalescence, and/or collision may be necessary, and extension of existing assembly theories and manipulation technologies and control strategies to droplet formation, drying and its response to external stimuli could be of a future research focus in fundamental science and application manufacturing technologies.

Acknowledgment

This work is supported by NSF-CMMI-1728149 and the University of Virginia.

Declaration of Competing Interest

The authors declare that they have no known competing financial interests or personal relationships that could have appeared to influence the work reported in this paper.

References

- 1. Winter C, Zettl M, Mantanus J et al. Development of a Workflow to Engineer Tailored Microparticles Via Inkjet Printing. *Pharmaceutical Research* 2023;40:281-294.
- 2. Liu Y, Zhu Y, Hu H, Guo T, Li F. Quantum dot self-assembly deposition in physically confined microscale space by using an inkjet printing technique. *The journal of physical chemistry letters* 2021;12:8605-8613.
- 3. Shao B, Wu X, Wang Y et al. A general method for selectively coating photothermal materials on 3D porous substrate surfaces towards cost-effective and highly efficient solar steam generation. *Journal of Materials Chemistry A* 2020;8:24703-24709.
- 4. Rousset N, Sandoval RL, Modena MM et al. Modeling and measuring glucose diffusion and consumption by colorectal cancer spheroids in hanging drops using integrated biosensors. *Microsystems & Nanoengineering* 2022;8:14.
- 5. Xu T, Xu LP, Zhang X, Wang S. Bioinspired superwettable micropatterns for biosensing. *Chemical Society reviews* 2019;48:3153-3165.
- 6. Kokornaczyk MO, Bodrova NB, Baumgartner SJC, Biointerfaces SB. Diagnostic tests based on pattern formation in drying body fluids—A mapping review. *Colloids and Surfaces B: Biointerfaces* 2021;208:112092.
- 7. Wang Y, Liu F, Yang Y, Xu L-P. Droplet evaporation-induced analyte concentration toward sensitive biosensing. *Materials Chemistry Frontiers* 2021;5:5639-5652.
- 8. Larson RG. Twenty years of drying droplets. *Nature* 2017;550:466-467.
- 9. Deegan RD. Pattern formation in drying drops. *Physical Review E* 2000;61:475-485.
- 10. Deegan RD, Bakajin O, Dupont TF et al. Capillary flow as the cause of ring stains from dried liquid drops. *Nature* 1997;389:827-829.
- 11. Hu H, Larson RG. Analysis of the effects of Marangoni stresses on the microflow in an evaporating sessile droplet. *Langmuir: the ACS journal of surfaces and colloids* 2005;21:3972-3980.
- 12. Hu H, Larson RG. Analysis of the microfluid flow in an evaporating sessile droplet. *Langmuir : the ACS journal of surfaces and colloids* 2005;21:3963-3971.
- 13. Gurrala P, Katre P, Balusamy S et al. Evaporation of ethanol-water sessile droplet of different compositions at an elevated substrate temperature. *International Journal of Heat and Mass Transfer* 2019;145:118770.
- 14. Gao A, Liu J, Ye L et al. Control of droplet evaporation on oil-coated surfaces for the synthesis of asymmetric supraparticles. *Langmuir*: the ACS journal of surfaces and colloids 2019;35:14042-14048.
- 15. Gregson FKA, Robinson JF, Miles REH, Royall CP, Reid JP. Drying and Crystallization of Evaporating Sodium Nitrate Aerosol Droplets. *The Journal of Physical Chemistry B* 2020;124:6024-6036.
- 16. Kuznetsova YV, Balyakin IA, Popov ID et al. Ag2S interparticle interaction in an aqueous solution: Mechanism of steric and electrostatic stabilization. *Journal of Molecular Liquids* 2021;335:116130.
- 17. Qiao Z, Gong X, Guan P et al. Lasing action in microdroplets modulated by interfacial molecular forces. *Advanced Photonics* 2021;3:016003.
- 18. Díaz-Marín CD, Li D, Vázquez-Cosme FJ et al. Capillary Transfer of Self-Assembled Colloidal Crystals. *Nano Letters* 2023.
- 19. Li X, Chen L, Ma Y et al. Ultrafast Fabrication of Large-Area Colloidal Crystal Micropatterns via Self-Assembly and Transfer Printing. *Advanced Functional Materials* 2022;32.
- 20. Shi S, Russell TP. Nanoparticle Assembly at Liquid-Liquid Interfaces: From the Nanoscale to Mesoscale. *Advanced materials* 2018;30:e1800714.

- 21. Shabani R, Kumar R, Cho HJ. Droplets on liquid surfaces: Dual equilibrium states and their energy barrier. *Applied Physics Letters* 2013;102.
- 22. Sebilleau J. Equilibrium thickness of large liquid lenses spreading over another liquid surface. Langmuir: the ACS journal of surfaces and colloids 2013;29:12118-12128.
- 23. Liu L, Jiang J, Zhang S et al. Morphology Evolution of a Volatile Liquid Lens on Another Immiscible Liquid Surface Induced by Evaporation. *Langmuir : the ACS journal of surfaces and colloids* 2021;37:14081-14088.
- 24. Sun W, Yang F. Evaporation of a Volatile Liquid Lens on the Surface of an Immiscible Liquid. *Langmuir: the ACS journal of surfaces and colloids* 2016;32:6058-6067.
- 25. Bird JC, Mandre S, Stone HA. Short-Time Dynamics of Partial Wetting. *Physical review letters* 2008;100:234501.
- 26. Biance A-L, Clanet C, Quéré D. First steps in the spreading of a liquid droplet. *Physical Review E* 2004;69:016301.
- 27. Carlson A, Do-Quang M, Amberg G. Dissipation in rapid dynamic wetting. *Journal of Fluid Mechanics* 2011;682:213-240.
- 28. Neumann FE. Vorlesungen über mathematische Physik: Vorlesungen über die Theorie des Potentials und der Kugelfunctionem. BG Teubner, 1887.
- 29. Cao Z, Dobrynin AV. Polymeric Droplets on Soft Surfaces: From Neumann's Triangle to Young's Law. *Macromolecules* 2015;48:443-451.
- 30. Pokhrel S, Mädler L. Flame-made Particles for Sensors, Catalysis, and Energy Storage Applications. *Energy & Fuels* 2020;34:13209-13224.
- 31. Meng X, Meng L, Gao Y, Li H. A comprehensive review on the spray cooling system employed to improve the summer thermal environment: Application efficiency, impact factors, and performance improvement. *Building and Environment* 2022;217:109065.
- 32. Lim T, Lee J, Lee J, Ju S. Detection of chemicals in water using a three-dimensional graphene porous structure as liquid-vapor separation filter. *Nano Research* 2017;10:971-979.
- 33. Archer J, Walker JS, Gregson FKA, Hardy DA, Reid JP. Drying Kinetics and Particle Formation from Dilute Colloidal Suspensions in Aerosol Droplets. *Langmuir : the ACS journal of surfaces and colloids* 2020;36:12481-12493.
- 34. Handscomb CS, Kraft M, Bayly AE. A new model for the drying of droplets containing suspended solids. *Chemical Engineering Science* 2009;64:628-637.
- 35. Both EM, Nuzzo M, Millqvist-Fureby A, Boom RM, Schutyser MAI. Morphology development during single droplet drying of mixed component formulations and milk. *Food Research International* 2018;109:448-454.
- 36. Liu Q, Huang J, Xu B. Evaporation-driven crumpling and assembling of two-dimensional (2D) materials: A rotational spring mechanical slider model. *Journal of the Mechanics and Physics of Solids* 2019;133.
- 37. Liu Q, Xu B. Solution Evaporation-Driven Crumpling and Assembling of Large-Accessible-Space, High-Mechanical-Strength Graphene/Carbon Nanotube Composite Nanoparticles. *ACS applied materials & interfaces* 2020;12:43058-43064.
- 38. Pramanik C, Gissinger JR, Kumar S, Heinz H. Carbon Nanotube Dispersion in Solvents and Polymer Solutions: Mechanisms, Assembly, and Preferences. *ACS Nano* 2017;11:12805-12816.
- 39. Yang ZJ, Wei JJ, Sobolev YI, Grzybowski BA. Systems of mechanized and reactive droplets powered by multi-responsive surfactants (vol 553, pg 313, 2018). *Nature* 2019;567:E11-E11.

- 40. Gu DH, Choi W, Son JS. Self-Assembly of Matchstick-Shaped Inorganic Nano-Surfactants with Controlled Surface Amphiphilicity. *JACS Au* 2022;2:2307-2315.
- 41. Wang D, Chen L, Feng X. Superhydrophobicity-mediated enhanced enzymatic kinetics and high-performance bioassays. *Droplet* 2023;2:e51.
- 42. Erbil HY, McHale G, Newton MI. Drop Evaporation on Solid Surfaces: Constant Contact Angle Mode. *Langmuir: the ACS journal of surfaces and colloids* 2002;18:2636-2641.
- 43. Zhang X, Wang J, Bao L et al. Mixed mode of dissolving immersed nanodroplets at a solid–water interface. *Soft Matter* 2015;11:1889-1900.
- 44. Gunjan MR, Raj R. Dynamic Roughness Ratio-Based Framework for Modeling Mixed Mode of Droplet Evaporation. *Langmuir: the ACS journal of surfaces and colloids* 2017;33:7191-7201.
- 45. Marin AG, Gelderblom H, Lohse D, Snoeijer JH. Order-to-disorder transition in ring-shaped colloidal stains. *Physical review letters* 2011;107:085502.
- 46. Gelderblom H, Diddens C, Marin A. Evaporation-driven liquid flow in sessile droplets. *Soft Matter* 2022;18:8535-8553.
- 47. van Gaalen RT, Wijshoff HMA, Kuerten JGM, Diddens C. Competition between thermal and surfactant-induced Marangoni flow in evaporating sessile droplets. *Journal of Colloid and Interface Science* 2022;622:892-903.
- 48. Parsa M, Harmand S, Sefiane K, Bigerelle M, Deltombe R. Effect of substrate temperature on pattern formation of nanoparticles from volatile drops. *Langmuir : the ACS journal of surfaces and colloids* 2015;31:3354-3367.
- 49. Lee HJ, Choi CK, Lee SH. Local heating effect on thermal Marangoni flow and heat transfer characteristics of an evaporating droplet. *International Journal of Heat and Mass Transfer* 2022;195:123206.
- 50. Chen J, Yang C, Mao Z. The interphase mass transfer in liquid–liquid systems with Marangoni effect. *The European Physical Journal Special Topics* 2015;224:389-399.
- 51. Gennes P-G, Brochard-Wyart F, Quéré D. Capillarity and wetting phenomena: drops, bubbles, pearls, waves. Springer, 2004.
- 52. Fuchs NA. Evaporation and droplet growth in gaseous media. Elsevier, 2013.
- 53. Bae J, Lee J, Zhou Q, Kim T. Micro-/Nanofluidics for Liquid-Mediated Patterning of Hybrid-Scale Material Structures. *Advanced materials* 2019;31:1804953.
- 54. Su M, Song Y. Printable Smart Materials and Devices: Strategies and Applications. *Chemical reviews* 2022;122:5144-5164.
- 55. Keum K, Kim JW, Hong SY et al. Flexible/Stretchable Supercapacitors with Novel Functionality for Wearable Electronics. *Advanced materials* 2020;32:2002180.
- 56. Zhang Y, Liu Q, Xu B. Self-Folding Mechanics of Surface Wettability Patterned Graphene Nanoribbons by Liquid Evaporation. *Journal of Applied Mechanics* 2017;85.
- 57. Liu Q, Gao Y, Xu B. Liquid evaporation-driven folding of graphene sheets. *Applied Physics Letters* 2016;108.
- 58. Liu Q, Xu B. Two- and three-dimensional self-folding of free-standing graphene by liquid evaporation. *Soft Matter* 2018;14:5968-5976.
- 59. Petsi AJ, Kalarakis AN, Burganos VN. Deposition of Brownian particles during evaporation of two-dimensional sessile droplets. *Chemical Engineering Science* 2010;65:2978-2989.
- 60. Kim H-S, Park SS, Hagelberg F. Computational approach to drying a nanoparticle-suspended liquid droplet. *Journal of Nanoparticle Research* 2011;13:59-68.
- 61. Zigelman A, Manor O. The deposition of colloidal particles from a sessile drop of a volatile suspension

- subject to particle adsorption and coagulation. Journal of Colloid and Interface Science 2018;509:195-208.
- 62. Mollaret R, Sefiane K, Christy JRE, Veyret D. Experimental and Numerical Investigation of the Evaporation into Air of a Drop on a Heated Surface. *Chemical Engineering Research and Design* 2004;82:471-480.
- 63. Vodolazskaya IV, Tarasevich YY. THE MODEL OF DRYING SESSILE DROP OF COLLOIDAL SOLUTION. *Modern Physics Letters B* 2011;25:1303-1310.
- 64. Tarasevich YY, Vodolazskaya IV, Isakova OP. Desiccating colloidal sessile drop: dynamics of shape and concentration. *Colloid and Polymer Science* 2011;289:1015-1023.
- 65. Crivoi A, Duan F. Three-dimensional Monte Carlo model of the coffee-ring effect in evaporating colloidal droplets. *Scientific reports* 2014;4:4310.
- 66. Zolotarev PA, Kolegov KS. Monte Carlo simulation of particle size separation in evaporating bidispersed colloidal droplets on hydrophilic substrates. *Physics of Fluids* 2022;34:017107.
- 67. Landry ES, Mikkilineni S, Paharia M, McGaughey AJH. Droplet evaporation: A molecular dynamics investigation. *Journal of Applied Physics* 2007;102:124301.
- 68. Fede P, Simonin O, Villedieu P. Monte-Carlo simulation of colliding particles or coalescing droplets transported by a turbulent flow in the framework of a joint fluid–particle pdf approach. *International Journal of Multiphase Flow* 2015;74:165-183.
- 69. Consolini L, Aggarwal SK, Murad S. A molecular dynamics simulation of droplet evaporation. *International Journal of Heat and Mass Transfer* 2003;46:3179-3188.
- 70. Liu Q, Gao Y, Xu B. Transferable, Deep-Learning-Driven Fast Prediction and Design of Thermal Transport in Mechanically Stretched Graphene Flakes. *ACS Nano* 2021;15:16597-16606.
- 71. McClure ER, Carey VP. Determining Parametric Effects for Droplet Evaporation on Nanoporous Superhydrophillic Surfaces Using Machine Learning Techniques. 2021.
- 72. Li Y-F, Sheng Y-J, Tsao H-K. Evaporation Stains: Suppressing the Coffee-Ring Effect by Contact Angle Hysteresis. *Langmuir : the ACS journal of surfaces and colloids* 2013;29:7802-7811.
- 73. Thokchom AK, Zhou Q, Kim D-J, Ha D, Kim T. Characterizing self-assembly and deposition behavior of nanoparticles in inkjet-printed evaporating droplets. *Sensors and Actuators B: Chemical* 2017;252:1063-1070.
- 74. Kuncicky DM, Velev OD. Surface-Guided Templating of Particle Assemblies Inside Drying Sessile Droplets. *Langmuir: the ACS journal of surfaces and colloids* 2008;24:1371-1380.
- 75. Wu J, Xia J, Lei W, Wang B-p. Generation of the smallest coffee-ring structures by solute crystallization reaction on a hydrophobic surface. *RSC Advances* 2013;3.
- 76. Still T, Yunker PJ, Yodh AG. Surfactant-induced Marangoni eddies alter the coffee-rings of evaporating colloidal drops. *Langmuir : the ACS journal of surfaces and colloids* 2012;28:4984-4988.
- 77. Chen R, Zhang L, Zang D, Shen W. Blood drop patterns: Formation and applications. *Advances in colloid and interface science* 2016;231:1-14.
- 78. Shen X, Ho C-M, Wong T-S. Minimal Size of Coffee Ring Structure. *The Journal of Physical Chemistry B* 2010;114:5269-5274.
- 79. Li Y, Diddens C, Segers T et al. Evaporating droplets on oil-wetted surfaces: Suppression of the coffeestain effect. *PNAS* 2020;117:16756-16763.
- 80. Orejon D, Sefiane K, Shanahan MER. Stick-Slip of Evaporating Droplets: Substrate Hydrophobicity and Nanoparticle Concentration. *Langmuir: the ACS journal of surfaces and colloids* 2011;27:12834-12843.
- 81. Moffat JR, Sefiane K, Shanahan MER. Effect of TiO2 Nanoparticles on Contact Line Stick-Slip Behavior of Volatile Drops. *The Journal of Physical Chemistry B* 2009;113:8860-8866.

- 82. Orejon D, Sefiane K, Shanahan ME. Stick-slip of evaporating droplets: substrate hydrophobicity and nanoparticle concentration. *Langmuir*: the ACS journal of surfaces and colloids 2011;27:12834-12843.
- 83. Reid RC, Merrill MH, Thomas JP. Stick–slip behavior during electrowetting-on-dielectric: polarization and substrate effects. *Microfluidics and Nanofluidics* 2020;24:77.
- 84. Herbaut R, Brunet P, Limat L, Royon L. Liquid spreading on cold surfaces: Solidification-induced stick-slip dynamics. *Physical Review Fluids* 2019;4:033603.
- 85. Bhardwaj R, Fang X, Somasundaran P, Attinger D. Self-assembly of colloidal particles from evaporating droplets: role of DLVO interactions and proposition of a phase diagram. *Langmuir : the ACS journal of surfaces and colloids* 2010;26:7833-7842.
- 86. Molchanov SP, Roldughin VI, Chernova-Kharaeva IA, Yurasik GA. Dependence of the structure of ring-shaped deposits resulting from evaporation of dispersion droplets on initial contact angle. *Colloid Journal* 2016;78:633-640.
- 87. Zhong X, Xie H, Duan F. Deposition patterns from evaporating sessile droplets with suspended mixtures of multi-sized and multi-species hydrophilic and non-adsorbing nanoparticles. *Applied Thermal Engineering* 2017;111:1565-1572.
- 88. Malla LK, Bhardwaj R, Neild A. Analysis of profile and morphology of colloidal deposits obtained from evaporating sessile droplets. *Colloids and Surfaces A: Physicochemical and Engineering Aspects* 2019;567:150-160.
- 89. Anyfantakis M, Baigl D. Manipulating the Coffee-Ring Effect: Interactions at Work. *Chemphyschem : a European journal of chemical physics and physical chemistry* 2015;16:2726-2734.
- 90. Seo C, Jang D, Chae J, Shin S. Altering the coffee-ring effect by adding a surfactant-like viscous polymer solution. *Scientific reports* 2017;7:500.
- 91. Kuang M, Wang L, Song Y. Controllable Printing Droplets for High-Resolution Patterns. *Advanced materials* 2014;26:6950-6958.
- 92. Al-Milaji KN, Radhakrishnan V, Kamerkar P, Zhao H. pH-modulated self-assembly of colloidal nanoparticles in a dual-droplet inkjet printing process. *Journal of Colloid and Interface Science* 2018;529:234-242.
- 93. Lee HH, Fu SC, Tso CY, Chao CYH. Study of residue patterns of aqueous nanofluid droplets with different particle sizes and concentrations on different substrates. *International Journal of Heat and Mass Transfer* 2017;105:230-236.
- 94. Kumar PL, Thampi SP, Basavaraj MG. Particle size and substrate wettability dependent patterns in dried pendant drops. *J Phys Condens Matter* 2021;33:024003.
- 95. Patil ND, Bange PG, Bhardwaj R, Sharma A. Effects of Substrate Heating and Wettability on Evaporation Dynamics and Deposition Patterns for a Sessile Water Droplet Containing Colloidal Particles. *Langmuir: the ACS journal of surfaces and colloids* 2016;32:11958-11972.
- 96. Chhasatia VH, Sun Y. Interaction of bi-dispersed particles with contact line in an evaporating colloidal drop. *Soft Matter* 2011;7:10135.
- 97. Amjad M, Yang Y, Raza G et al. Deposition pattern and tracer particle motion of evaporating multi-component sessile droplets. *Journal of Colloid and Interface Science* 2017;506:83-92.
- 98. Bansal L, Seth P, Murugappan B, Basu S. Suppression of coffee ring: (Particle) size matters. *Applied Physics Letters* 2018;112:211605.
- 99. Chatterjee S, Murallidharan JS, Bhardwaj R. Size-dependent dried colloidal deposit and particle sorting via saturated alcohol vapor-mediated sessile droplet spreading. *Langmuir : the ACS journal of surfaces and colloids* 2022;38:6128-6147.

- 100. Das S, Dey A, Reddy G, Sarma DD. Suppression of the Coffee-Ring Effect and Evaporation-Driven Disorder to Order Transition in Colloidal Droplets. *The journal of physical chemistry letters* 2017;8:4704-4709.
- 101. Askounis A, Sefiane K, Koutsos V, Shanahan MER. The effect of evaporation kinetics on nanoparticle structuring within contact line deposits of volatile drops. *Colloids and Surfaces A: Physicochemical and Engineering Aspects* 2014;441:855-866.
- 102. Eral HB, Augustine DM, Duits MHG, Mugele F. Suppressing the coffee stain effect: how to control colloidal self-assembly in evaporating drops using electrowetting. *Soft Matter* 2011;7.
- 103. He P, Derby B. Controlling coffee ring formation during drying of inkjet printed 2D inks. *Advanced Materials Interfaces* 2017;4:1700944.
- 104. Baldwin KA, Roest S, Fairhurst DJ, Sefiane K, Shanahan ME. Monolith formation and ring-stain suppression in low-pressure evaporation of poly (ethylene oxide) droplets. *Journal of fluid mechanics* 2012;695:321-329.
- 105. Sefiane K, Wilson S, David S, Dunn G, Duffy B. On the effect of the atmosphere on the evaporation of sessile droplets of water. *Physics of fluids* 2009;21:062101.
- 106. Ghassemi H, Baek SW, Khan QS. Experimental study on binary droplet evaporation at elevated pressures and temperatures. *Combustion science technology* 2006;178:1031-1053.
- 107. Lim SX, Ren J, Ong K-S, Chong KSL, Duan F. Evaporation-driven octagonal particle deposition on the patterned substrate. *Droplet* 2022;1:202-213.
- 108. Inanlu MJ, Shojaan B, Farhadi J, Bazargan V. Effect of particle concentration on surfactant-induced alteration of the contact line deposition in evaporating sessile droplets. *Langmuir: the ACS journal of surfaces and colloids* 2021;37:2658-2666.
- 109. Shao X, Duan F, Hou Y, Zhong X. Role of surfactant in controlling the deposition pattern of a particle-laden droplet: Fundamentals and strategies. *Advances in colloid interface science* 2020;275:102049.
- 110. Li C, Pei J, Ye X. Spreading of droplet with insoluble surfactant on corrugated topography. *Physics of Fluids* 2014;26:092103.
- 111. Tamano S, Ohashi Y, Morinishi Y. Dynamics of falling droplet and elongational properties of dilute nonionic surfactant solutions with drag-reducing ability. *Physics of Fluids* 2017;29.
- 112. Gao Y, Yin M, Zhang H, Xu B. Electrically Suppressed Outflow of Confined Liquid in Hydrophobic Nanopores. *ACS Nano* 2022;16:9420-9427.
- 113. Yang M, Chen D, Hu J et al. The application of coffee-ring effect in analytical chemistry. *TrAC Trends in Analytical Chemistry* 2022:116752.
- 114. Zhang J, Borg MK, Ritos K, Reese JM. Electrowetting Controls the Deposit Patterns of Evaporated Salt Water Nanodroplets. *Langmuir : the ACS journal of surfaces and colloids* 2016;32:1542-1549.
- 115. Jeong H, van Tiem J, Gianchandani YB, Park J. Nano-Particle Separation Using Marangoni Flow in Evaporating Droplets. 2014 Solid-State, Actuators, and Microsystems Workshop Technical Digest, 2014:223-226.
- 116. Langmuir I. Oil Lenses on Water and the Nature of Monomolecular Expanded Films. *The Journal of Chemical Physics* 1933;1:756-776.
- 117. Burton JC, Huisman FM, Alison P, Rogerson D, Taborek P. Experimental and numerical investigation of the equilibrium geometry of liquid lenses. *Langmuir*: the ACS journal of surfaces and colloids 2010;26:15316-15324.
- 118. Rahman MR, Mullagura HN, Kattemalalawadi B, Waghmare PR. Droplet spreading on liquid–fluid interface. *Colloids and Surfaces A: Physicochemical and Engineering Aspects* 2018;553:143-148.

- 119. Liu L, Xu C, Zhao L, Mi M, Li C. Experimental and Theoretical Study of Evaporation of a Volatile Liquid Lens on an Immiscible Liquid Surface. *Langmuir : the ACS journal of surfaces and colloids* 2019;35:12979-12985.
- 120. Guan JH, Wells GG, Xu B et al. Evaporation of Sessile Droplets on Slippery Liquid-Infused Porous Surfaces (SLIPS). *Langmuir : the ACS journal of surfaces and colloids* 2015;31:11781-11789.
- 121. Xiao R, Miljkovic N, Enright R, Wang EN. Immersion condensation on oil-infused heterogeneous surfaces for enhanced heat transfer. *Scientific reports* 2013;3:1-6.
- 122. Upot NV, Rabbi KF, Khodakarami S et al. Advances in micro and nanoengineered surfaces for enhancing boiling and condensation heat transfer: a review. *Nanoscale Advances* 2023.
- 123. Guo Z, Monga D, Shan L, Boylan D, Dai X. Coarsening-induced disappearing droplets contribute to condensation. *Droplet* 2022;1:170-181.
- 124. Li W, Ji W, Lan D, Wang Y. Self-Assembly of Ordered Microparticle Monolayers from Drying a Droplet on a Liquid Substrate. *The journal of physical chemistry letters* 2019;10:6184-6188.
- 125. Singha P, Swaminathan S, Yadav AS, Varanakkottu SN. Surfactant-Mediated Collapse of Liquid Marbles and Directed Assembly of Particles at the Liquid Surface. *Langmuir: the ACS journal of surfaces and colloids* 2019:35:4566-4576.
- 126. Pham T, Kumar S. Imbibition and evaporation of droplets of colloidal suspensions on permeable substrates. *Physical Review Fluids* 2019;4:034004.
- 127. Pack M, Hu H, Kim D-O, Yang X, Sun Y. Colloidal Drop Deposition on Porous Substrates: Competition among Particle Motion, Evaporation, and Infiltration. *Langmuir: the ACS journal of surfaces and colloids* 2015;31:7953-7961.
- 128. Dou R, Derby B. Formation of Coffee Stains on Porous Surfaces. *Langmuir : the ACS journal of surfaces and colloids* 2012;28:5331-5338.
- 129. Hardy D, Archer J, Lemaitre P et al. High time resolution measurements of droplet evaporation kinetics and particle crystallisation. *Physical Chemistry Chemical Physics* 2021;23:18568-18579.
- 130. Strizhak P, Volkov R, Castanet G et al. Heating and evaporation of suspended water droplets: Experimental studies and modelling. *International Journal of Heat Mass Transfer* 2018;127:92-106.
- 131. Iskandar F, Gradon L, Okuyama K. Control of the morphology of nanostructured particles prepared by the spray drying of a nanoparticle sol. *Journal of Colloid and Interface Science* 2003;265:296-303.
- 132. Agthe M, Plivelic TS, Labrador A, Bergström L, Salazar-Alvarez G. Following in Real Time the Two-Step Assembly of Nanoparticles into Mesocrystals in Levitating Drops. *Nano Letters* 2016;16:6838-6843.
- 133. Zhang S, Campagne C, Salaün F. Preparation of Electrosprayed Poly(caprolactone) Microparticles Based on Green Solvents and Related Investigations on the Effects of Solution Properties as Well as Operating Parameters. *Coatings*, 2019.
- 134. Huynh E, Olinger A, Woolley D et al. Evidence for a semisolid phase state of aerosols and droplets relevant to the airborne and surface survival of pathogens. *Proceedings of the National Academy of Sciences* 2022;119:e2109750119.
- 135. Shi Q, Di W, Dong D et al. A General Approach to Free-Standing Nanoassemblies via Acoustic Levitation Self-Assembly. *ACS Nano* 2019;13:5243-5250.
- 136. Dubey P, Gopinath P. Fabrication of electrospun poly (ethylene oxide)—poly (capro lactone) composite nanofibers for co-delivery of niclosamide and silver nanoparticles exhibits enhanced anti-cancer effects in vitro. *Journal of Materials Chemistry B* 2016;4:726-742.
- 137. Tang J, Gomez A. Controlled mesoporous film formation from the deposition of electrosprayed nanoparticles. *Aerosol Science and Technology* 2017;51:755-765.

- 138. Yang J, Sun H, Liang H et al. A Highly Efficient Metal-Free Oxygen Reduction Electrocatalyst Assembled from Carbon Nanotubes and Graphene. *Advanced materials* 2016;28:4606-4613.
- 139. Luo J, Jang HD, Sun T et al. Compression and Aggregation-Resistant Particles of Crumpled Soft Sheets. *ACS Nano* 2011;5:8943-8949.
- 140. Tang C, Liu L, Li Y, Bian Z. Aerosol spray assisted assembly of TiO2 mesocrystals into hierarchical hollow microspheres with enhanced photocatalytic performance. *Applied Catalysis B: Environmental* 2017;201:41-47.
- 141. Alagh A, Annanouch FE, Umek P et al. CVD growth of self-assembled 2D and 1D WS2 nanomaterials for the ultrasensitive detection of NO2. *Sensors and Actuators B: Chemical* 2021;326:128813.
- 142. Zhang H, Moon SK, Ngo TH. 3D Printed Electronics of Non-contact Ink Writing Techniques: Status and Promise. *International Journal of Precision Engineering and Manufacturing-Green Technology* 2019;7:511-524.
- 143. Kwon J-S, Lee D, Oh J. Formation and Characterization of Inkjet-Printed Nanosilver Lines on Plasma-Treated Glass Substrates. *Applied Sciences* 2018;8.
- 144. Antonopoulou E, Harlen OG, Rump M, Segers T, Walkley MA. Effect of surfactants on jet break-up in drop-on-demand inkjet printing. *Physics of Fluids* 2021;33:072112.
- 145. Tsai MH, Hwang WS, Chou HH, Hsieh PH. Effects of pulse voltage on inkjet printing of a silver nanopowder suspension. *Nanotechnology* 2008;19:335304.
- 146. Aqeel AB, Mohasan M, Lv P, Yang Y, Duan H. Effects of nozzle and fluid properties on the drop formation dynamics in a drop-on-demand inkjet printing. *Applied Mathematics and Mechanics* 2019;40:1239-1254.
- 147. Ma S, Ribeiro F, Powell K et al. Fabrication of Novel Transparent Touch Sensing Device via Drop-on-Demand Inkjet Printing Technique. *ACS applied materials & interfaces* 2015;7:21628-21633.
- 148. Dang CM, Huynh KK, Dang DMT. Influence of Solvents on Characteristics of Inkjet Printing Conductive Ink Based on Nano Silver Particles. *Biological Chemical Research* 2019;6:126-134.
- 149. Ding H, He P, Yang J et al. Water-based highly conductive graphene inks for fully printed humidity sensors. *Journal of Physics D: Applied Physics* 2020;53:455304.
- 150. Suntornnond R, Ng WL, Huang X, Yeow CHE, Yeong WY. Improving printability of hydrogel-based bio-inks for thermal inkjet bioprinting applications via saponification and heat treatment processes. *Journal of Materials Chemistry B* 2022;10:5989-6000.
- 151. Kang S-H, Kim S, Sohn DK, Ko HS. Analysis of drop-on-demand piezo inkjet performance. *Physics of Fluids* 2020;32:022007.
- 152. Kwon H-j, Hong J, Nam SY et al. Overview of recent progress in electrohydrodynamic jet printing in practical printed electronics: Focus on the variety of printable materials for each component. *Materials Advances* 2021;2:5593-5615.
- 153. Vasiljević DZ, Mansouri A, Anzi L, Sordan R, Stojanović GM. Performance Analysis of Flexible Ink-Jet Printed Humidity Sensors Based on Graphene Oxide. *IEEE Sensors Journal* 2018;18:4378-4383.
- 154. Nge TT, Nogi M, Suganuma K. Electrical functionality of inkjet-printed silver nanoparticle conductive tracks on nanostructured paper compared with those on plastic substrates. *Journal of Materials Chemistry C* 2013;1:5235-5243.
- 155. Park JU, Lee S, Unarunotai S et al. Nanoscale, electrified liquid jets for high-resolution printing of charge. *Nano Lett* 2010;10:584-591.
- 156. Barmpakos D, Tsamis C, Kaltsas G. Multi-parameter paper sensor fabricated by inkjet-printed silver nanoparticle ink and PEDOT:PSS. *Microelectronic Engineering* 2020;225:111266.

- 157. Hu H, Chen Q-W, Tang J, Hu X-Y, Zhou X-H. Photonic anti-counterfeiting using structural colors derived from magnetic-responsive photonic crystals with double photonic bandgap heterostructures. *Journal of Materials Chemistry* 2012;22.
- 158. Han S, Bae HJ, Kim J et al. Lithographically Encoded Polymer Microtaggant Using High-Capacity and Error-Correctable QR Code for Anti-Counterfeiting of Drugs. *Advanced materials* 2012;24:5924-5929.
- 159. Chen L, Zhang Y, Luo A et al. The temperature-sensitive luminescence of (Y,Gd)VO4:Bi3+,Eu3+ and its application for stealth anti-counterfeiting. *physica status solidi (RRL) Rapid Research Letters* 2012;6:321-323.
- 160. Nam H, Song K, Ha D, Kim T. Inkjet Printing Based Mono-layered Photonic Crystal Patterning for Anti-counterfeiting Structural Colors. *Scientific reports* 2016;6:30885.
- 161. Liu Y, Li F, Qiu L et al. Fluorescent Microarrays of in Situ Crystallized Perovskite Nanocomposites Fabricated for Patterned Applications by Using Inkjet Printing. *ACS Nano* 2019;13:2042-2049.
- 162. Feng C, Zheng X, Xu R et al. Highly efficient inkjet printed flexible organic light-emitting diodes with hybrid hole injection layer. *Organic Electronics* 2020;85:105822.
- 163. Mizukami M, Cho SI, Watanabe K et al. Flexible Organic Light-Emitting Diode Displays Driven by Inkjet-Printed High-Mobility Organic Thin-Film Transistors. *IEEE Electron Device Letters* 2018;39:39-42.
- 164. Kong X, Xi Y, LeDuff P et al. Optofluidic sensing from inkjet-printed droplets: the enormous enhancement by evaporation-induced spontaneous flow on photonic crystal biosilica. *Nanoscale* 2016;8:17285-17294.
- 165. Zhu Y, Zhang Y-X, Liu W-W et al. Printing 2-Dimentional Droplet Array for Single-Cell Reverse Transcription Quantitative PCR Assay with a Microfluidic Robot. *Scientific reports* 2015;5:9551.
- 166. Qin Y, Kwon H-J, Subrahmanyam A et al. Inkjet-printed bifunctional carbon nanotubes for pH sensing. *Materials Letters* 2016;176:68-70.
- 167. Heng W, Pang G, Xu F et al. Flexible Insole Sensors with Stably Connected Electrodes for Gait Phase Detection. *Sensors*, 2019.
- 168. Bihar E, Wustoni S, Pappa AM et al. A fully inkjet-printed disposable glucose sensor on paper. *npj Flexible Electronics* 2018;2:30.
- 169. Fu E, Wentland L. A survey of 3D printing technology applied to paper microfluidics. *Lab on a Chip* 2022;22:9-25.
- 170. Zhou W, Dou M, Timilsina SS, Xu F, Li X. Recent innovations in cost-effective polymer and paper hybrid microfluidic devices. *Lab on a Chip* 2021;21:2658-2683.
- 171. Nasir A, Yatabe R, Mikami Y et al. Ink-jet printed, blended polymer-based microdisk resonators for controlling non-specific adsorption of biomolecules. *Optics Letters* 2021;46:262-265.
- 172. Zhou X, Zhou Y, Ku JC, Zhang C, Mirkin CA. Capillary force-driven, large-area alignment of multi-segmented nanowires. *ACS nano* 2014;8:1511-1516.
- 173. Guo HW, Hu Z, Liu ZB, Tian JG. Stacking of 2D materials. *Advanced Functional Materials* 2021;31:2007810.
- 174. Ye H, Yin C, Wang J, Zheng Y. Controllable and Gradient Wettability of Bilayer Two-Dimensional Materials Regulated by Interlayer Distance. *ACS Applied Materials Interfaces* 2022;14:41489-41498.

ToC figure:

Droplet drying provides a low-cost and facile route for assembling materials and structures in a wide spectrum of functionalities down to the nanoscale and also serves as a basis for innovating ink-solution based future printing technologies. The fundamental mechanics theories that are underpinned for material assembly by droplet drying on solid and liquid substrates and in a fully suspended air environment, along with the challenges and future opportunities, are highlighted with representative applications in printing electronic devices.

Ziyu Chen, Kangyi Peng, Baoxing Xu*

Material assembly by droplet drying: from mechanics theories to applications

